Journal of Energy Chemistry 90 (2024) 40–57

Contents lists available at ScienceDirect

Journal of Energy Chemistry

journal homepage: www.elsevier.com/locate/jechem

http://www.journals.elsevier.com/journal-of-energy-chemistry/

Review

Difficulties, strategies, and recent research and development of layered sodium transition metal oxide cathode materials for high-energy sodium-ion batteries

Kouthaman Mathiyalagan [a], Dongwoo Shin [b], Young-Chul Lee [b,*]

[a] Department of Nano Science and Technology Convergence, Gachon University, 1342 Seongnam-Daero, Sujeong-Gu, Gyeonggi-Do, Seongnam-Si 13120, Republic of Korea
[b] Department of BioNano Technology, Gachon University, 1342 Seongnam-Daero, Sujeong-Gu, Gyeonggi-Do, Seongnam-Si 13120, Republic of Korea

ARTICLE INFO

Article history:
Received 23 August 2023
Revised 13 October 2023
Accepted 15 October 2023
Available online 26 October 2023

Keywords:
O3-type
P2-type
Cathode materials
Sodium-ion batteries
Layered structure

ABSTRACT

Energy-storage systems and their production have attracted significant interest for practical applications. Batteries are the foundation of sustainable energy sources for electric vehicles (EVs), portable electronic devices (PEDs), etc. In recent decades, Lithium-ion batteries (LIBs) have been extensively utilized in large-scale energy storage devices owing to their long cycle life and high energy density. However, the high cost and limited availability of Li are the two main obstacles for LIBs. In this regard, sodium-ion batteries (SIBs) are attractive alternatives to LIBs for large-scale energy storage systems because of the abundance and low cost of sodium materials. Cathode is one of the most important components in the battery, which limits cost and performance of a battery. Among the classified cathode structures, layered structure materials have attracted attention because of their high ionic conductivity, fast diffusion rate, and high specific capacity. Here, we present a comprehensive review of the classification of layered structures and the preparation of layered materials. Furthermore, the review article discusses extensively about the issues of the layered materials, namely (1) electrochemical degradation, (2) irreversible structural changes, and (3) structural instability, and also it provides strategies to overcome the issues such as elemental phase composition, a small amount of elemental doping, structural design, and surface alteration for emerging SIBs. In addition, the article discusses about the recent research development on layered unary, binary, ternary, quaternary, quinary, and senary-based O3- and P2-type cathode materials for high-energy SIBs. This review article provides useful information for the development of high-energy layered sodium transition metal oxide P2 and O3-cathode materials for practical SIBs.
© 2023 Science Press and Dalian Institute of Chemical Physics, Chinese Academy of Sciences. Published by ELSEVIER B.V. and Science Press. All rights reserved.



Kouthaman Mathiyalagan received his B.Sc. degree in Department of Physics from H.H. The Rajah's college, Pudukkottai, Tamilnadu, India, in 2013 and M.Sc. degree in Department of Physics from Alagappa University, Karaikudi, Tamilnadu, India, in 2015. Furthermore, he received his M.Phil. degree in Department of Physics from Alagappa University, Karaikudi, Tamilnadu, India, in 2016 and Ph.D. in Department of Physics from Alagappa University, Karaikudi, Tamilnadu, India, in 2022. Currently, he is working as an assistant professor in the Department of Nano Science and Technology convergence, Gachon University, South Korea, from April 2023. His research interest mainly focuses on developing high-energy cathode materials with low-cost for emerging sodium-ion batteries.



Dongwoo Shin received his Bachelor's degree in Department of BioNano Technology, Gachon University, Republic of Korea, from February 2023. Currently, he is working as a senior researcher in the Corporate R&D Center, PUROM Co., LTD from March 2023. Also, he is still collaborating as a researcher in the Department of BioNano Technology, Gachon University. His research interest is synthesizing alloy materials for anodes in lithium-ion and sodium-ion batteries, especially on synthesizing novel anode and cathode materials, based on aminoclay structures. Additionally, he is developing water-borne epoxy coating agent in order to use a binder.

* Corresponding author.
E-mail address: dreamdbs@gachon.ac.kr (Y.-C. Lee).

https://doi.org/10.1016/j.jechem.2023.10.023
2095-4956/© 2023 Science Press and Dalian Institute of Chemical Physics, Chinese Academy of Sciences. Published by ELSEVIER B.V. and Science Press. All rights reserved.



Young-Chul Lee received his Master and PhD degree in Chemical & Biomolecular. Engineering from Korea Advanced Institute & Science Technology (KAIST), Daejeon in February 2011. From 2011 to 2013, he worked as a postdoctoral researcher in Department of Chemical and Biochemical Engineering, Chosun University and KAIST. Then he worked as a research professor from 2013 to 2014 in Inha University, South Korea. Currently, he is working as an associate professor in the Department of BioNano Technology, Gachon University, South Korea, in from April 2014. His research interests are inorganic-organic nanoparticles, especially on antioxidant or redox nanoparticles(sub-nanoparticles) for biological, environmental and cosmetic applications using aminoclays, hydrogels and 2D layered materials. In addition, his research is focusing on cathode and anode materials for sodium-ion batteries.

1. Introduction

Due to the need for energy sources and rising energy consumption, the demand for high efficiency, low maintenance, long cycle life, proper protection, renewable energy, and low cost has increased with regard to energy storage systems. Rechargeable batteries are the best professional representations among various electrical energy storage systems for storing energy and providing power for electric automobiles and portable electronic devices. In 1990, the SONY company commercialized lithium-ion batteries (LIBs) invented by Prof. J. B. Goodenough using graphitic material as the anode and layered $LiCoO_2$ as the cathode [1–4]. LIBs have been significantly improved and widely used in the fields of power grid storage, electric vehicles, and personal electronic devices owing to their long cycle life, high energy density, specific capacity, low self-discharge rate, and environmental friendliness. Nevertheless, high prices and low availability of lithium resources are major challenges for LIBs [5–8]. In this regard, room-temperature sodium-ion batteries (SIBs) have attracted increasing interest and are considered to be one of the most promising solutions for energy storage systems because of their rich natural abundance, worldwide distribution, and working mechanism similar to that of LIBs, in addition to the low cost of sodium materials [9–12].

Recent investigations on SIBs have focused on the growth of electrode materials. The anode materials are classified into three types for SIBs: conversion, alloying, and intercalation. In addition, Anode materials have achieved significant improvements in terms of rate capability and capacity to date. Cathode materials play a vital role in determining the lifetimes and energy densities of SIBs. Generally, cathode materials for SIBs are classified into three types: Prussian blue analogues, Polyanion compounds, and Layered transition metal oxides (Fig. 1) [13–18]. Prussian blue analogues are favorable cathode materials with excellent electrochemical performance for SIBs, although they exhibit temperature instability and low tap densities during electrochemical reactions. Furthermore, a low tap density affects the energy density of battery systems [19,20]. Polyanion-type based compounds have a strong covalent bond between the oxygen polyhedron (MO_x) and transition metal, which can create a structure, composed of a three-dimensional framework or two-dimensional van der Waals bonding, leading to quick alkali ion movement paths. Furthermore, it exhibits small volume changes, oxidation stabilities when charging and discharging, thermal stabilities, and tunable operating voltages by inducing local environments of polyanions, etc. However, high operating voltages, which may affect electrolyte stability, poor electronic conductivities, and complicated synthesis process are the main challenges for SIBs [21,22].

Finally, layered transition metal oxides (Na_xTMO_2, (x = 0 to 1, TM = Mn, Ni, Fe, Co, Ti, etc.)) are promising and have undergone substantial research as cathode materials for SIBs because of their high specific capacity, high ionic conductivity, easy synthesis process, simple structure, and environmental benignity. The layered structure promoted the rapid migration of sodium ions owing to its distinctive 2D diffusion pathway. Moreover, the cation disorder diminishes between the transition metal ions and sodium ions than Lithium Li^+ (0.67 Å) owing to the greater size of sodium ions Na^+ (1.02 Å). Compared to olivine and spinel, layered cathode materials are a promising solution for high-performance SIBs [1,23–25].

Previously, Liu et al. [1] extensively investigated that the single, binary, ternary, and multi metal oxides, full cell, and battery manufacture of the layered sodium transition metal cathodes for SIBs. Xiao et al. [14] comprehensively explored that the morphology design, coating technology, phase transition and suppression, air stability, and composite structure of the layered oxide cathodes for SIBs. Furthermore, Wei et al. [26] meticulously explored that the single, binary, ternary, and multi component based O3 and P2-types, and hybrid structure (P&O) of the layered transition metal oxide cathode materials for SIBs. Besides, Liu et al. [27] widely examined that the anionic redox activity, sodium-rich oxide cathodes, sodium deficient oxide cathodes, mixed phase cathodes of the layered transition metal oxides for SIBs. However this article systematically scrutinized the classification of structure, synthesis procedures, and issues & tactics of the layered cathode materials for SIBs. In addition, the recent research progress on unary, binary, ternary, quaternary, quinary, and senary based O3 and P2-type cathode materials also discussed in detail.

In this review, we provide a brief overview of the most recent advancements in the study of layered sodium transition-metal oxides, particularly, layered O3- and P2-type cathode materials, for SIBs. In particular, we focus on the structural classification, design of the materials, the problems with the layered structure, and several strategies for enhancing electrochemical performance. Layered sodium transition metal oxides (Na_xTMO_2) are powerful candidates for SIBs owing to their attractive properties.

2. Classification of layered crystal structure

In the 1980s, two-dimensional layered transition metal oxides (Na_xTMO_2) were evaluated by Hagenmuller and Delmas. Generally, Alkali ions are stacked between layers of oxygen to form layered structures. Polymorphisms were produced when sheets of edge-sharing MeO_6 octahedra were placed along the c-axis in different directions. Layered Na transition metal oxides can be classified into four types: O3, P2, O2, and P3. The numbers 3 and 2 represent the number of transition metal oxide (TMO_2) layers with various types of oxygen arrangements in each unit cell. The symbols O and P denote the location of alkali ions (Na^+) in the structure, where O denotes that the sodium ions are located in the octahedral location between the TMO_2 layers, and P denotes that the sodium ions are situated on the prismatic site between the TMO_2 layers. The stacking sequences of the oxygen layers in the O3, P2, O2, and P3 structures were ABCABC, ABBA, ABAC, and ABBCCA, respectively, as shown in Fig. 2(a–d). Besides, the prime symbol (′) denotes the monoclinic distortion in the crystal structure. For example, P′3 and O′3 signify the monoclinic distortion of the P3 and O3-phases, respectively.

In the O3-type phase, the TMO_6 octahedra and Na^+ ions in the crystal structures are associated in an edge-sharing manner. When the x-value of Na_xTMO_2 is high (x near 1), the O3-type structure is stable. The transition metal and sodium ions are located at distinct octahedral positions in the cubic close-packed oxygen array of the O3-type phase, and the ionic radius of transition metal ions (<0.7 Å) is substantially smaller than that of sodium ions (1.02 Å). Edge-shared TMO_6 octahedra and NaO_6 sequence into alternative layers along the [111] direction in O3-type materials, creating TMO_2 and NaO_2 slabs, respectively. The three separate

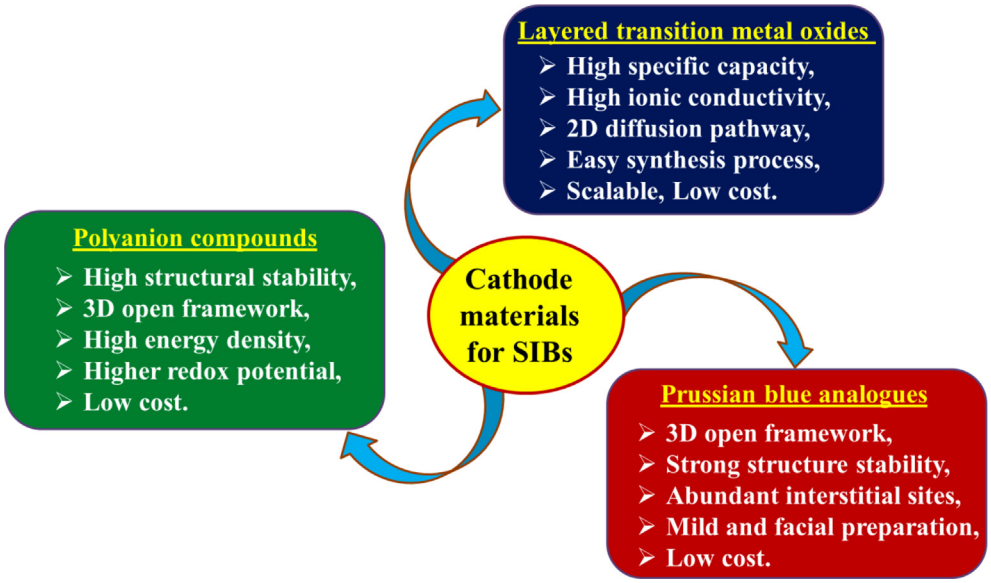


Fig. 1. Schematic illustration of types of cathode materials for SIBs.

TMO_2 layers, AB, CA, and BC, comprise a layered O3-type structure, which is categorized as a 3R phase with the space group R-3m. Generally, O3-type materials have higher sodium concentrations than P2-type materials, making them ideal for full-battery applications.

The phase transition from O3 or P3 to P2 is not possible during electrochemical reactions in sodium cells because a high-temperature heat treatment is necessary to break the TM-O bonds and form the P2 phase. Additionally, O3-type materials commonly undergo this O3-P3 phase transition during cycling and do not break any O bonds. Vacancies are created in the crystal structures when sodium ions are partially eliminated, which promotes an energetically favorable prismatic environment, increasing the interlayer distance as a result of the strong oxygen repulsion caused by this extraction in the sodium layers. Moreover, sodium ions diffusion occurred more quickly in the P3 phase owing to the increased interlayer distance than in the O3 phase. Hence, O3-type materials frequently undergo complicated phase transitions, leading to poor capacity retention, inadequate rate capability, and severe structural deterioration. These disadvantages hinder the use of O3-type materials in SIBs.

The TMO_6 octahedra and sodium ions in the crystal structures are connected in an edge-and-face-sharing manner in the P2-type phase. When the sodium concentration in Na_xTMO_2 is in the range ($0.3 \leq X \leq 0.7$), the P2-type structure is stable. The P2-type layered structure includes two different types of TMO_2 layers, AB and BA, and is categorized as the 2H phase with the space group P63/mmc. Na1 (Na_e) and Na2 (Na_f) are two different types of trigonal prismatic sites where sodium ions occur in the P2-type. Along its edges, Na1 associates with two of the adjacent slabs of the TMO_6 octahedra, whereas along its faces, Na2 associates with the six surrounding TMO_6 octahedra. Furthermore, owing to the gliding of some TMO_6 octahedra sheets (π /3 rotation), the P2 phase typically transforms into the O2 phase, and when charged at a relatively greater voltage, the crystal structure is significantly shrunk, and the interlayer distance is reduced. The P2 to O2 phase change leads to a severe capacity reduction and large volume change (~20%) during electrochemical reactions. Thus, it is crucial to determine how to enhance the structural stability of P2-type materials [26–39].

There are three distinct TMO_2 layers AB, BC, and CA oxygen stacking in the P3-type phase with a space group of R-3m. The P2-type phase often forms after high-temperature calcination at approximately 900 °C, whereas the P3-type phase is typically formed under low-temperature calcination, for example, at approximately 700 °C. Therefore, it can be assumed that the P3-type cathode uses less energy. During the charge and discharge processes, the P2-type and P3-type phases contained the same Na positions as the prismatic sites, whereas the O3-type phase always transformed into the P3-type phase. Furthermore, layered P3-type materials exhibit an improved cycle life and rate performance compared with O3-type materials because P3-type layered materials have almost the same outstanding structural durability as P2-type materials. In addition, P3-type phase-layered materials have greater sodium content and discharge capability than P2-type phase materials. However, when electrochemical reactions occur, P3-type phase materials experience significant capacity decay because of their asymmetric crystal systems. Additionally, because of the large ionic radius of Na, the structure of the layered P3-type phase is affected throughout the cycling process. In addition, most layered-structured materials exhibit a poor cycle life because the lattice oxygen of the layered materials is irreversibly converted into oxygen [31,40–44].

3. Synthesis procedures of layered structure materials for SIBs

The material-preparation procedure is critical for developing crystal shapes that can be used in high-performance SIBs. Several material preparation methods are available, such as hydrothermal, classical solid-state reaction, polyol, co-precipitation, sol–gel, combustion, solvothermal, and spray-drying methods, to attain phase purity, particle size, electrochemical performance, and the desired morphology. Furthermore, the sodium ratio plays an important role in the formation of O3 and P2-type layered structured materials (Na_xTMO_2). In common, the O3-type structure is typically formed if $x > 0.7$ and P2-type structure is usually formed if $x < 0.7$. Generally, a solid-state reaction is widely utilized as a synthesis method because of its easy preparation procedure and simple operation. For instance, Leng et al. [45] reported that the

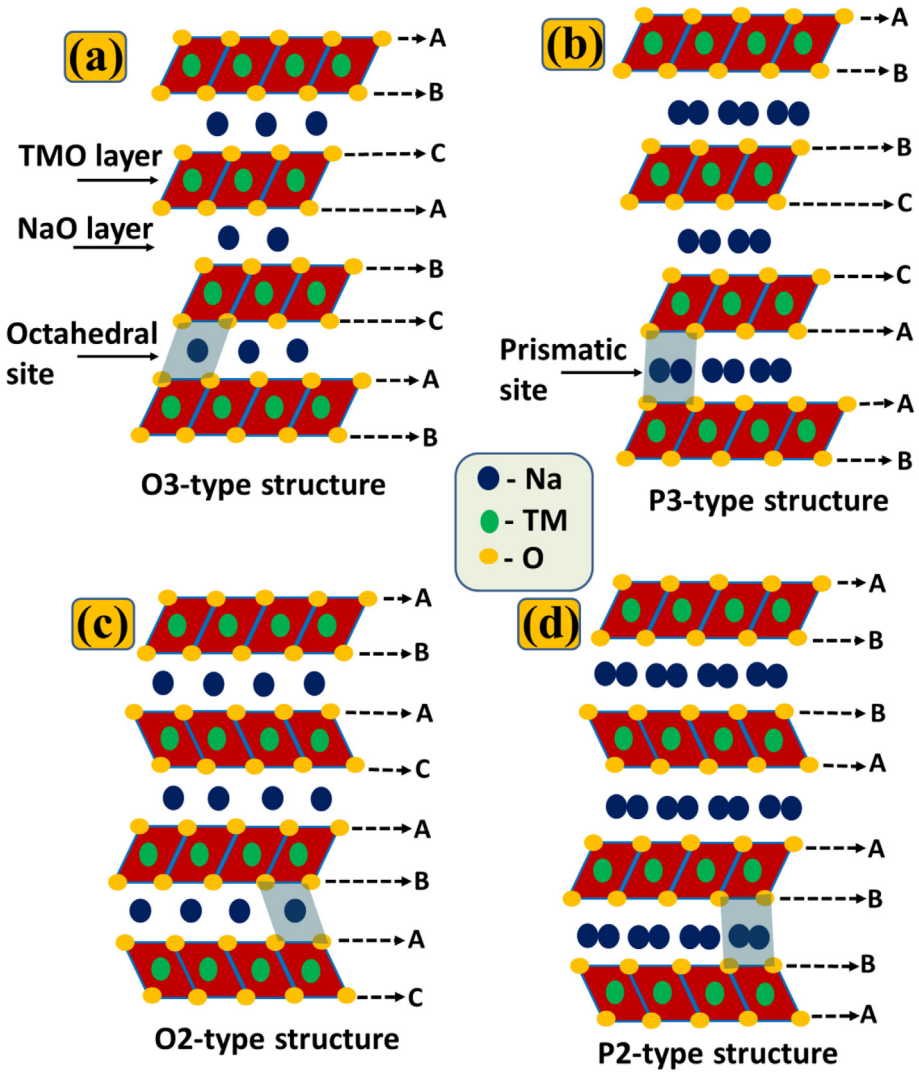


Fig. 2. Schematic illustrations of the layered structure (a) O3-structure, (b) P3-structure, (c) O2-structure, and (d) P2-structure.

stoichiometric amounts of Na_2CO_3, MnO_2, TiO_2, NiO, and RuO_2 were grounded using a pestle and mortar, and using a high-temperature furnace, the mixed powder was calcined at 900 °C for 12 h under air environment. Finally, the layered O3-Na $Mn_{0.3}Ni_{0.48}Ru_{0.02}Ti_{0.2}O_2$ cathode material was obtained. The prepared cathode material delivered discharge capacity was 155.3 mA h g^{-1} in the voltage range of 1.5–4.5 V at a 0.05 C rate. Hu et al. [46] and Zhang et al. [28] prepared P2-type $Na_{0.67}Cu_{0.1}Ni_{0.225}Mn_{0.675}O_2$ and O3-type Na $Ni_{0.2}Mn_{0.48}Mg_{0.02}Fe_{0.3}O_2$ layered cathode materials via conventional solid-state reactions. Furthermore, to understand how the type and level of elemental doping affect the electrochemical performance of materials, the traditional high-temperature solid-state method is extremely useful. However, in the solid-state method, the calcination conditions and choice of precursors, particularly the calcination temperature, significantly affect the material. Additionally, this method makes it difficult to manage the morphology and particle size of the materials, which cannot entirely achieve atomic-level uniformity. Therefore, a solution method was applied to prepare cathode materials with fine particle sizes and controllable morphologies.

To lower production costs and achieve high uniformity, the sol–gel process is an excellent option for high-performance materials. Stoichiometric amounts of the starting material were dissolved in distilled water and mixed with citric acid in a sol–gel process. Citric acid was used as the chelating agent. The resultant mixture was stirred at 80 °C to gradually transition to the sol–gel state. The obtained gels were then heated for 12 h at 120 °C. Subsequently, the dried gels were ground, sintered for five hours at 500 °C, and then calcined for 12 h at 900 °C in the air using a furnace to produce the final products. Li et al. [47] synthesized a layered P2-type $Mn_{0.8}Na_{0.67}Mg_{0.1}Ni_{0.1}O_2$ cathode material via the sol–gel method with a discharge capacity of 124 mA h g^{-1}. A small amount of co-substitution enhanced the structural and cycling stability of the material. Material preparation using this method has a low manufacturing cost. However, because of its exceedingly slow reaction time, industrial production is highly challenging [48–50].

The polyol method is a unique approach that allows for easy access to nanoparticles with tailored shapes, sizes, and compositions. In the polyol method, a stoichiometric molar ratio of the starting materials is dissolved in a polyol solvent, such as diethylene glycol. After 18 h, the solution was heated in a refluxed condenser to a temperature close to the boiling point of the polyol solvent. The resulting solution was washed several times with acetone, deionized water, and ethanol to remove the polyol solvent and other organic compounds. The resulting particles were then heated in a vacuum oven for 48 h at 150 °C. Finally, the resulting powder was calcined at 600 °C for 1 h under an argon atmosphere

in a high-temperature furnace to produce the final products. Nanoparticle synthesis using this method is the most effective; however, the material preparation period is too long and is very difficult for industrial manufacture [51–53].

The co-precipitation method is a standard process for high-performance materials because of its higher uniformity, more controlled morphology, and consistent particle size. In the co-precipitation method, the preparation of cathode materials typically involves two processes. First, stoichiometric amounts of the raw materials were dissolved in deionized water to prepare a 1 M aqueous solution. Subsequently, the carbonate precursor was dissolved in deionized water with ammonium hydroxide to form another solution. The two solutions were simultaneously added to a beaker at 60 °C for 12 h, using a syringe pusher. The pH of the solution was maintained at this value. Subsequently, the resulting precipitate was separated and rinsed several times with deionized water. The obtained precursor was heated in a vacuum oven for 12 h at 100 °C. The dried precursors were then mixed with a carbonate source. Finally, to produce the finished product, the mixed precursors were heated at 600 °C for 6 h and then calcined at 900 °C for 12 h in air [54–56]. Co-precipitation was used by Zhang et al. [57] to create a layered P2-$Na_{0.56}[Co_{0.1}Mn_{0.8}Ni_{0.1}]O_2$ cathode material that offered outstanding rate performance and long-term cyclability for SIBs, as well as a high discharge capacity of 188 mA h g^{-1}. The prepared cathode material was more controlled in terms of size and morphology than the solid-state approach and exhibited greater homogeneity. However, the co-precipitation approach is particularly challenging because of its high synthesis cost and strict synthesis processes.

The hydrothermal method is a unique process that allows easy access to nanoparticles of tailored sizes and compositions. Stoichiometric amounts of raw materials were dissolved in deionized water and stirred. The mixed solution was then transferred to a Teflon-lined autoclave and heated to 180 °C for 12 h to undergo hydrothermal treatment. The resulting solution was filtered, rinsed repeatedly with ethanol and deionized water, and dried in an oven at 100 °C for 12 h. Subsequently, to prepare for the outcome, the resulting powder was pre-calcined at 300 °C for 3 h and then further calcined at 650 °C for 6 h in an air atmosphere [58,59]. Alam et al. [60] synthesized a layered O3-type $NaMg_xFe_{1-x}O_2F$ (x = 0.5) cathode material using a hydrothermal method, which offered excellent cycling durability and a high discharge capacity of 171.35 mA h g^{-1} for SIBs. Furthermore, Kaliyappan et al. [61] prepared a layered P2-type $Na_{0.66}(Ni_{0.13}Co_{0.13}Mn_{0.54})O_2$ material using a hydrothermal method, which offered excellent rate performance and improved cycling stability with uniform size distribution and shape during the charge and discharge processes. However, Teflon-lined autoclaves are expensive and difficult to produce industrially.

The combustion method is a typical process for high-performance materials owing to its speed, simplicity, low energy consumption, and lack of special equipment. A stoichiometric amount of the raw material was dissolved in deionized water. Glycine was used as the fuel for the combustion reaction and was added to the solution. The mixture was heated to 100 °C and stirred for 12 h to form a viscous slurry that evaporated water. The viscous slurry was then combusted at 300 °C for 1 h in a furnace. To obtain the final product, the resultant powder was calcined at 600 °C for 6 h in the air in a muffle furnace [62–67]. Nanthagopal et al. [68] prepared a layered O3-type $NaMn_{0.5}Fe_{0.5}O_2$ cathode material via a combustion method that provided a high discharge capacity of 188 mA h g^{-1} along with low-cost and earth-abundant SIBs. Kumar et al. [69] synthesized a small amount of transition metal substituted O3-$NaCo_{0.18}Mn_{0.3}Al_{0.02}Ni_{0.5}O_2$ layered cathode material via the combustion method, which increased the structural stability and promoted electrochemical performance, with 90% capacity retention at a 0.1 C rate after 200 cycles. In addition, a small quantity of Al substitution enhanced the bond strength between TM and O and increased the number of NaO_2 layers. Therefore, Na ions are easily intercalated during the electrochemical reaction between the positive and negative electrodes. Nonetheless, the main disadvantages are the existence of a moderately large quantity of carbon in the final product and poor control of the morphology and combustion process.

The solvothermal method is also a standard method for high-performance materials owing to its composition control, ease of synthesis, and regulation of the resultant particle properties, such as size, shape, high surface area, and dispersion. In the solvothermal method, a stoichiometric amount of the starting material was dissolved in a mixed solvent of ethylene glycol and deionized water. Urea was used as the nucleating agent for the solvothermal method and was added to the solution. The mixture was then placed in a Teflon-lined autoclave and heated for 24 h at 200 °C. The resulting solution was rinsed multiple times with ethanol, acetone, and deionized water before drying in a vacuum oven at 80 °C for 12 h. To obtain the final product, the powder was calcined at 900 °C for 12 h in an Ar environment in a high-temperature furnace [70–72]. Xiao et al. [73] prepared a layered P2-type $Na_{0.66}Mn_{0.71}Co_{0.08}Li_{0.18}Mg_{0.21}O_2$ cathode material via the solvothermal method, which provided excellent capacity retention and a high discharge capacity of 166 mA h g^{-1}. Additionally, the structural and cycle stabilities of the synthesized materials were enhanced by substituting a small amount of transition metal in the TMO layers. However, the main disadvantages of this approach are the high temperature and expensive equipment.

To create a mixed solution, a stoichiometric amount of the starting material was dissolved in deionized water and stirred continuously using the spray drying method. The resulting mixed solution was dried using a spray dryer to obtain a powder. During the spray-drying process, the inlet and outlet temperatures were 200 and 100 °C, respectively, with a spraying speed of 250 mLh^{-1}. Finally, the spray-dried powders are pre-heated at 300 °C for three hours and then further calcined at 600 °C for six hours in an argon atmosphere using a high-temperature furnace [74–76]. Qin et al. [77] prepared O3-type layered $NaNi_{1/3-0.005}Zn_{0.005}Mn_{1/3}Fe_{1/3}O_2$ cathode material via the spray-drying method, which gives 123 mA h g^{-1} of the discharge capacity with 87% capacity retention at a 1 C rate after 200 cycles. During high-voltage cycling, a small amount of Zn substitution in the TMO layer efficiently prevented the formation of cracks and oxygen loss and enhanced the rate capability and cycling stability of the prepared materials. Moreover, Wang et al. [78] synthesized a P2-$Na_{2/3}[Mn_{2/3}Ni_{1/3}]O_2$ cathode material using a spray-drying method, and the prepared cathode material exhibited superior reversibility between 2 and 4 V with long-term cyclability. The main drawbacks of this method are its fast drying times, ease of operation, and suitability for mass production. However, spray dryers have several limitations.

Each approach has its unique relative benefits and a variety of effects on the morphology, shape, purity, and size of the materials, as well as a variety of requirements for production costs and the environment. Consequently, preparation methods have been continuously developed to generate superior layered transition metal materials.

4. Issues of layered structure materials

In layered structures, three important issues occur during charge and discharge processes: electrochemical degradation, irreversible structural changes, and structural instability (Fig. 3). The side reactions with the electrolyte in the aforementioned first instance affect the electrochemical performance of the materials.

In the second instance, O3, O'3, O'3, and P3 phase transitions often occur in O3-type materials during electrochemical reactions, whereas P2 and O2 phase transitions normally occur in P2-type materials. The phase transitions of the materials were observed using in situ (X-ray diffraction). Furthermore, because of this irreversible phase change, the cathode materials suffer from capacity loss and structural degradation. Third, laminate materials are extremely sensitive to the environment, which means that airborne CO_2 and moisture affect them. The following section discusses the main problems associated with layered-structure materials with these features.

4.1. Electrochemical degradation

Water corrosion and irreversible structural changes occur in layer-structured materials, which restrict the reversible capacity and cause rapid capacity fading during the electrochemical reaction. The electrochemical properties of layered cathode materials are currently inadequate for large-scale energy-storage applications for the aforementioned reasons. In particular, Mn-based layered materials have some drawbacks, such as rapid capacity degradation and structural strain caused by Jahn–Teller high-spin Mn^{3+} during the charge and discharge processes, and there is a chance that Mn ions could dissolve in the electrolyte, although they have low polarization and a high initial reversible capacity. Furthermore, if Mn has the valence state Mn^{3+}, the Mn–O bond will extend in a particular direction, and significant structural distortions will be caused by this crystal structure asymmetry. Moreover, after the sodium ions are eliminated from the solid matrix, vacancies appear, providing locations for H/H_2O insertion to generate a protonated phase.

For the aforementioned reasons, the Na-ion diffusion pathway could be obstructed, significantly reducing the Na-ion diffusion coefficient [79–81]. Han et al. [82] evaluated a layered P2-type $Na_{2/3}Mn_{0.8}Ti_{0.1}Fe_{0.1}O_2$ cathode material for high-rate SIBs using a ceramic technique. The prepared pristine cathode material exhibited superior electrochemical performance, with a capacity retention of 88% after the 2nd cycle. Simultaneously, the moisture-exposed cathode material exhibited a capacity retention of 70%, which is very low compared with that of the pristine cathode material.

4.2. Irreversible structural changes

Generally, during the charge and discharge processes, O3– and P2-type structured materials undergo a series of phase changes caused by the extraction of sodium ions from the sites, including various stacking arrangements of the oxygen layers. The P2-type phase is generally transformed into the O2-type phase during electrochemical reactions because of the sliding of the TMO_6 octahedral layers with sodium ion extraction. Because of these issues, the crystal structure shrinks significantly, and the distance between the layers is reduced. Furthermore, irreversible P2-O2 phase transitions at high voltages cause rapid capacity deterioration and structural collapse of P2-type layered materials. Moreover, compared to P2-type structures, the O3-type phase typically experiences more complicated phase changes, such as structural transitions of O3 to P3, P'3, and O'3 during the sodiation/de-sodiation process. Na first stabilizes at the TMO_6 octahedral location, which is shared via the edges in the O3-type phase. When the Na ions were partially removed in the O3-type phase and vacancies were formed, the Na in the middle of the prism became energy stable. Subsequently, a wide prism center was created by sliding the TMO_2 sheet without rupturing the TM—O bonds. Consequently, the typical stacking of the oxygen layers (O3-type phase) changed from ABCABC to ABBCCA. This phenomenon is known as the P3-type phase.

Yao et al. [83] evaluated a layered O3-type $NaFe_{0.45}Mg_{0.05}Co_{0.5}O_2$ cathode material prepared via a simple solid-state reaction that frequently underwent more complex phase changes, for example, from O3 to P3, P'3, and O'3, as evidenced by in situ XRD. In a study by Liu et al. [84], a P2-type layered $Na_{2/3}Mn_{2/3}Ni_{1/3}O_2$ cathode material was synthesized using the sol–gel technique, which suffers from a single-phase transformation of P2 to O2, and the phase change was identified using in situ XRD. Additionally, owing to the single-phase change, the P2-type layered materials sustain better structural and cycling stability than the O3-type layered materials during the cycling proess. However, owing to their lower sodium content, layered P2-type materials have a lower reversible capacity than O3-type materials. Hence, owing to their low diffusion barrier and moral structural integrity, P2-type layered materials consistently demonstrate moral cycling durability and rate capability compared to O3-type materials [85–88].

4.3. Structural instability

The layered materials typically reveal poor air stability due to surface sensitivity to environmental surroundings and ease of insertion of the air moisture, apart from the structural transformations and sluggish kinetics. In terms of air stability, the reaction processes of water on various crystal structures of layered oxide cathode materials are different. For example, in the P2 type structure, water molecules can insert into the sodium layer to generate a $Na_xTMO_2.yH_2O$ hydrate phase. Nonetheless, layered structure (Na_xTMO_2) phase can be regenerated through heat treatment to remove the water molecules [14].

Recently, Zuo et al. [89] prepared layered P2-type $Na_{0.67}MnO_2$ and P2-$Na_{0.67}Mn_{0.67}Ni_{0.33}O_2$ cathode materials for SIBs via classical solid-state reactions. Moreover, using various characterization techniques, such as in situ XRD, TOF-SIMS, solid-state NMR, and first-principles calculations, the chemical and structural degradation mechanisms of the prepared layered cathode materials were

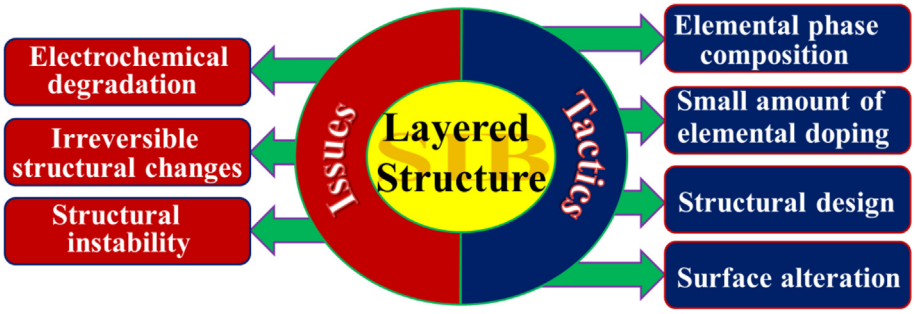


Fig. 3. Main issues and tactics of the layered materials for SIBs.

thoroughly examined in diverse ambient atmospheres. Furthermore, Xu et al. [90] reported that the insertion of CO_2 into the Na layers along the (003) planes of Na_xTMO_2 led to the initial formation of Na_2CO_3 nano seeds between the TM layers (layered-structure materials). This initiates the extrusion of Na_2CO_3 from Na_xTMO_2 and rapid structural degradation with surface cracks. In addition, the particle shape, crystal orientation, and ambient humidity were significantly associated with the extent and path of Na_xTMO_2 degradation. Surprisingly, degraded layered-structure materials can be entirely modified via optimum recalcination, resulting in enhanced air stability and electrochemical properties.

5. Tactics of layered structure materials

Recently, many researchers have evaluated methods to solve these three main issues. To improve the electrochemical performance of cathode materials with a layered structure, four key strategies are available: elemental phase composition, a small amount of elemental doping, structural design, and surface alteration (Fig. 3). During sodiation and de-sodiation, a small amount of elemental doping is regularly used to inhibit irreversible structural transformations. To reduce the side reactions that occur between the electrolyte and particle surface, surface modification is performed, and it is possible to protect the layered material from atmospheric CO_2 and humidity. Researchers can modify the phase and structure of electrode materials to obtain suitable cathode materials.

5.1. Elemental phase composition

To date, most studies have evaluated the P2, O3, and P3 phases in layered cathode materials. Owing to the irreversible phase changes, the initial Coulombic efficiency is lower in P2-type materials. However, the sodium-ion diffusion rates are higher in the P2-type layered materials. Layered P3-type structured materials have greater interlayer spacing than P2-type structured materials, which provides broader pathways for sodium ion diffusion and exhibits enhanced rate performance. Furthermore, layered O3-type structural materials have higher sodium content but poor cycling properties during the cycling process. Therefore, researchers have devoted attention to studying better structures to obtain excellent electrochemical performance. By incorporating the advantages of the different phases, a composite material was obtained that provides a novel approach for obtaining new layered cathode materials with good electrochemical performance.

For instance, Zhang et al. [91] synthesized a layered P3/O3 biphasic $Na_{2/3}Mn_{1/3}Ti_{1/3}Ni_{1/3}O_2$ cathode material for SIBs using the sol–gel method. The capacity retention of 69% at 0.1 C after 2000 cycles in the voltage range of 2.5–4.15 V with outstanding cycling performance and high rate capability is provided by the P3/O3 biphasic cathode materials. Liang et al. [92] prepared layered P2-$Na_{2/3}Mn_{2/3}Ni_{1/3}O_2$ (NM), co-doped $Na_{2/3}Ni_{2/9}Mn_{5/9}Fe_{1/9}Mg_{1/9}O_2$ (NMFM), and $Na_{7/9}Ni_{2/9}Fe_{1/9}Mn_{4/9}Li_{1/9}Mg_{1/9}O_2$ (NMFML) cathode materials via classical solid-state reactions for high-energy SIBs. The novel P2/O3 biphasic NMFML cathode material successfully suppresses destructive P2-O2 phase changes, alleviating internal stress at high voltages during electrochemical cycling. Because of the combination of the stabilizing dopant materials (Li, Mg, and Fe) and suppressed dissolution of active materials, the prepared NMFML cathode material exhibited improved Na-ion diffusion kinetics and enhanced structural durability. After 500 cycles, the NMFML cathode material had an excellent capacity retention of 72% at 1 C, a superior rate capability of 106.6 mA h g^{-1} at 10 C, and a high initial discharge capacity of 170.5 mA h g^{-1} (Fig. 4a–i). In addition, several layered biphasic-based cathode materials have been incorporated, such as P2/O3 biphasic $Na_{0.67}Mg_{0.15}Mn_{0.425}Fe_{0.425}O_2$ [93], P2/O3 $Na_{0.8}Fe_{0.2}Li_{0.2}Mn_{0.6}O_2$ [94], P2 + O3 type $Na_{0.66}Mn_{0.71}Li_{0.18}Co_{0.08}Ni_{0.21}O_{2+\delta}$ composites [95], P2/O3-phase $Na_{2/3}Mn_{0.8}Li_{0.18}Fe_{0.2}O_2$ [96], P2/P3 biphasic $Na_{0.7}Mn_{0.67}Li_{0.06}Ni_{0.22}Mg_{0.06}O_2$ [97], P2/O3 biphasic $Na_{0.7}Fe_{0.36}Li_{0.11}Mn_{0.36}Ti_{0.17}O_2$ [98]. Moreover, it provides an innovative method for enhancing the performance of layered materials by combining the distinct benefits of various phases. Although there are particular benefits to this modification technique, it is necessary to further study the mechanism of interactions between various phases and the preparation of composite materials.

5.2. Small amount of elemental doping

Because transition metal ions undergo irreversible migration during the charge and discharge processes, the transition metal ions in the layered structure can degrade their performance. This may lead to irreversible structural transformations and distortions of the materials. To solve these problems, a minimum amount of electrochemically active/inactive transition metals (for example, Ti, Mg, Al, Zn, Cu, F, and Li, etc.) doping into TMO layers (Na_xTMO_2) has been demonstrated to be beneficial. The doping ions are classified into two types: cations and anions. Doping with a small amount of transition metals has been demonstrated to be useful for many-layered cathode materials owing to its enhanced structural and cycling stability, enhanced rate performance, increased long-term stability, and improved operating voltage. Anion doping is commonly used for polyanions, whereas cation doping is used for both layered materials and polyanions. Furthermore, cation doping is effective in generating predictable results only in a small number of cases; however, anion doping has been shown to have few side effects [99,100].

5.2.1. Cationic doping

Cationic doping is used to avoid irreversible phase changes and improve the electrochemical properties of layered materials. The connection between TM and O can be strengthened to some extent by sharing oxygen with other transition metal elements, and the Jahn-Teller distortion can be reduced to some extent by doping. Hence, the phase changes were inhibited, and the mobility of TMO_6 was reduced. Hu et al. [46] prepared a minimum quantity of Cu-doped P2-$Na_{0.67}Cu_{0.1}Ni_{0.225}Mn_{0.675}O_2$ cathode material for SIBs via a classical solid-state reaction. Owing to the minimum quantity of Cu doping in the Mn site, the percentage of Mn^{3+} is diminished, which alleviates Teller distortion. Therefore, the cathode material has better structural stability and rate capability. In addition, phase transitions and Na^+/vacancy ordering changes were further inhibited by Cu doping at high voltages during the electrochemical reaction. Consequently, the capacity retention and high-rate performance of the prepared materials were improved.

Generally, P2-type layered-structure materials have a higher interlayer spacing than O3-type layered-structure materials; this is associated with the greater conductivity of sodium ions during the discharge and charge processes. The interlayer spacing of the layered materials was adjusted by elemental doping. Hou et al. [48] prepared layered P2-type $Na_{0.67}Mn_{0.67}Ni_{0.33}O_2$ and a small amount of Mg-substituted manganese-based ($Na_{0.67}Mg_{0.1}Mn_{0.67}Ni_{0.23}O_2$) cathode as promising SIBs. Owing to the shrinkage of the TMO_6 octahedra and the reduction of the TM-O bond lengths caused by Mg doping, the Na-ion diffusion layer expands during cycling. Accordingly, sodium ions were easily intercalated during the electrochemical reaction owing to the increased NaO_2 layer thickness and the decrease in the TMO_2 layer thickness (Fig. 5a and b). After 100 cycles, the Mg-doped $Na_{0.67}Mg_{0.1}Ni_{0.23}Mn_{0.67}O_2$ cathode material sustained a discharge capacity of 85 mA g^{-1} and demonstrated an initial discharge capacity of 105 mA h g^{-1}.

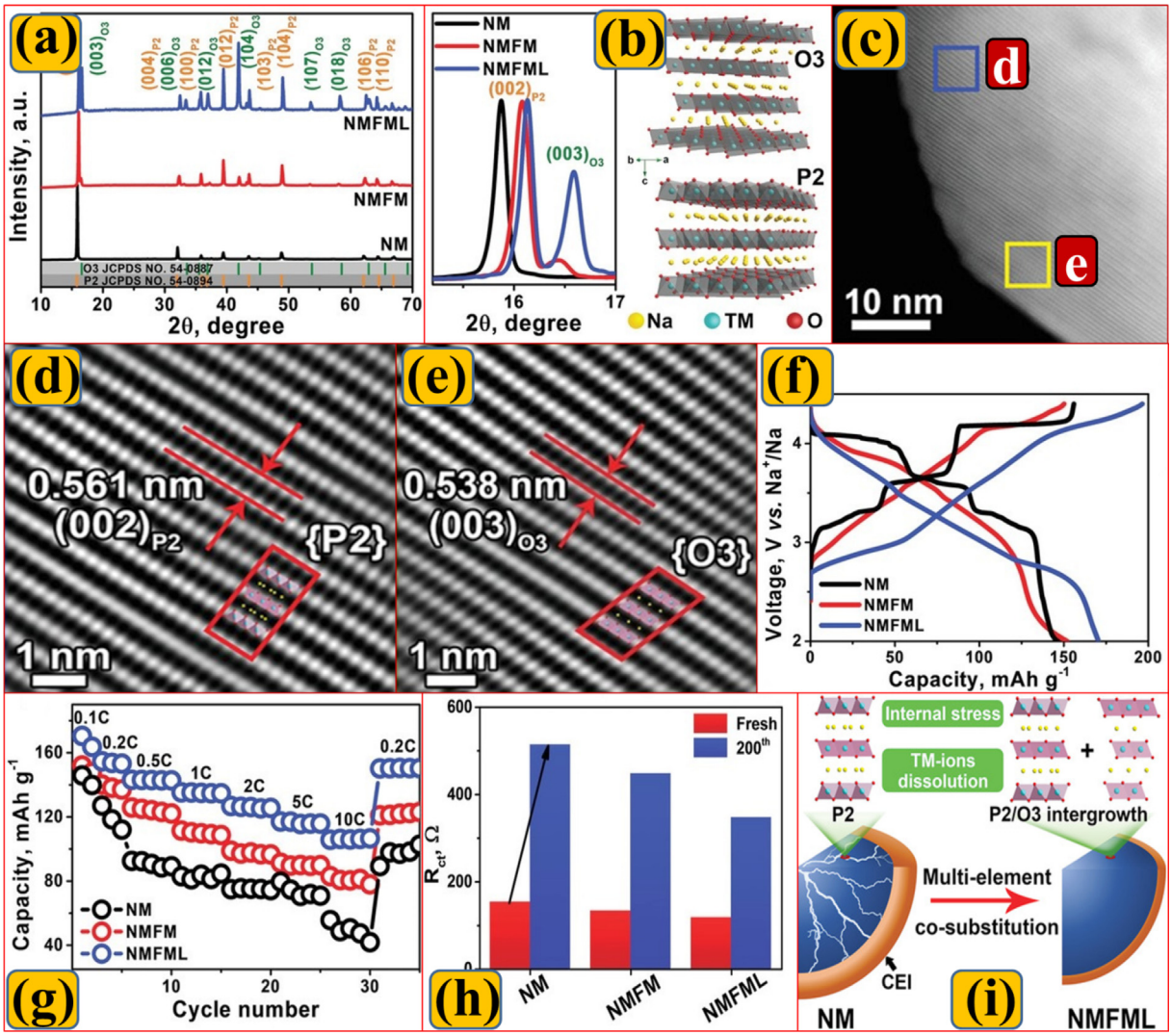


Fig. 4. (a) XRD patterns of NMFML, NMFM, and NM, (b) crystal representation of O3-phase (top) and P2-phase (bottom), (c–e) HR-TEM images of NMFML, (f) initial discharge / charge curves, (g) rate capability at various current rates from 0.1 to 10 C, (h) charge transfer resistance (R_{ct}) of NMFML, NMFM, and NM cathodes before and after 200 cycles, and (i) structural evolution of NMFML and NM cathodes during electrochemical reaction. Reproduced with permission from Ref. [92]. Copyright 2022, Wiley-VCH.

Without the Mg-doped cathode, the discharge capacity was high, but the cycling stability was poor, as shown in Fig. 5(c). Therefore, a minimum amount of Mg doping in the TMO layers enhanced the structural stability, cycling durability, and rate capability of the prepared cathode materials cycling [47].

Moreover, titanium (Ti) is a superior substituent for enriching the electrochemical performance of layered-structure materials compared to electrochemically inactive elements such as Mg and Al, owing to the significant total charge variation that contributes to capacity [101]. The layered P2-type $Na_{0.5}Ni_{0.25}Ti_{0.15}Mn_{0.60}O_2$ cathode material was prepared and its electrochemical performance was examined in detail by Zhang et al. [102]. The structural stability of the synthesized cathode material was improved using the least amount of Ti doping at the Mn sites, which prevented Mn^{3+} dissolution and Jahn-Teller distortion. The doping of Ti by inhibiting Na^+ vacancy ordering can smooth the charge and discharge curves between the voltage ranges of 2–4 V. Besides, the P2 and O2 phase changes of the prepared layered cathode materials at high voltages can be prevented using the least amount of Ti doping. Therefore, doping with a small amount of a transition metal (Ti) significantly enhances the structural and cycling stability and improves the rate performance of the prepared layered P2-type cathode material for SIBs [103–105].

5.2.2. Anionic doping

Another approach for tailoring layered cathode materials proposed in SIBs involves doping with various anions, such as S, Cl, and F. Li et al. [106] scrutinized P3-type $Na_{0.5}Mn_{0.75}Ni_{0.25}O_2$ layered materials for SIBs for the first time. This exhibited the viability of the insertion of cations (Na^+) and anions (ClO_4^-) into layered materials. In addition, the anion contribution provided partial charge compensation for the entire cell redox process, which was kinetically rapid and maintained. This idea provides innovative concepts for increasing reversible capacities. Consequently, the lowest amount of doping can reduce cation fraternization, reduce oxygen release, prevent irreversible oxygen loss, effectively enrich ionic conductivity, improve structural immovability, and improve the electrochemical properties of cathode materials [107,108].

Wang et al. [41] synthesized layered P3-$Na_{0.65}Ni_{0.25}Mn_{0.75}O_2$ (NaMNO), F (fluorine)-doped P3-$Na_{0.65}Ni_{0.25}Mn_{0.75}F_{0.1}O_{1.9}$ (NaMNO-F), and B (boron)-doped P3-$Na_{0.65}Ni_{0.25}Mn_{0.75}B_{0.1}O_2$ (NaMNO-B) cathode materials using a hydrothermal method for

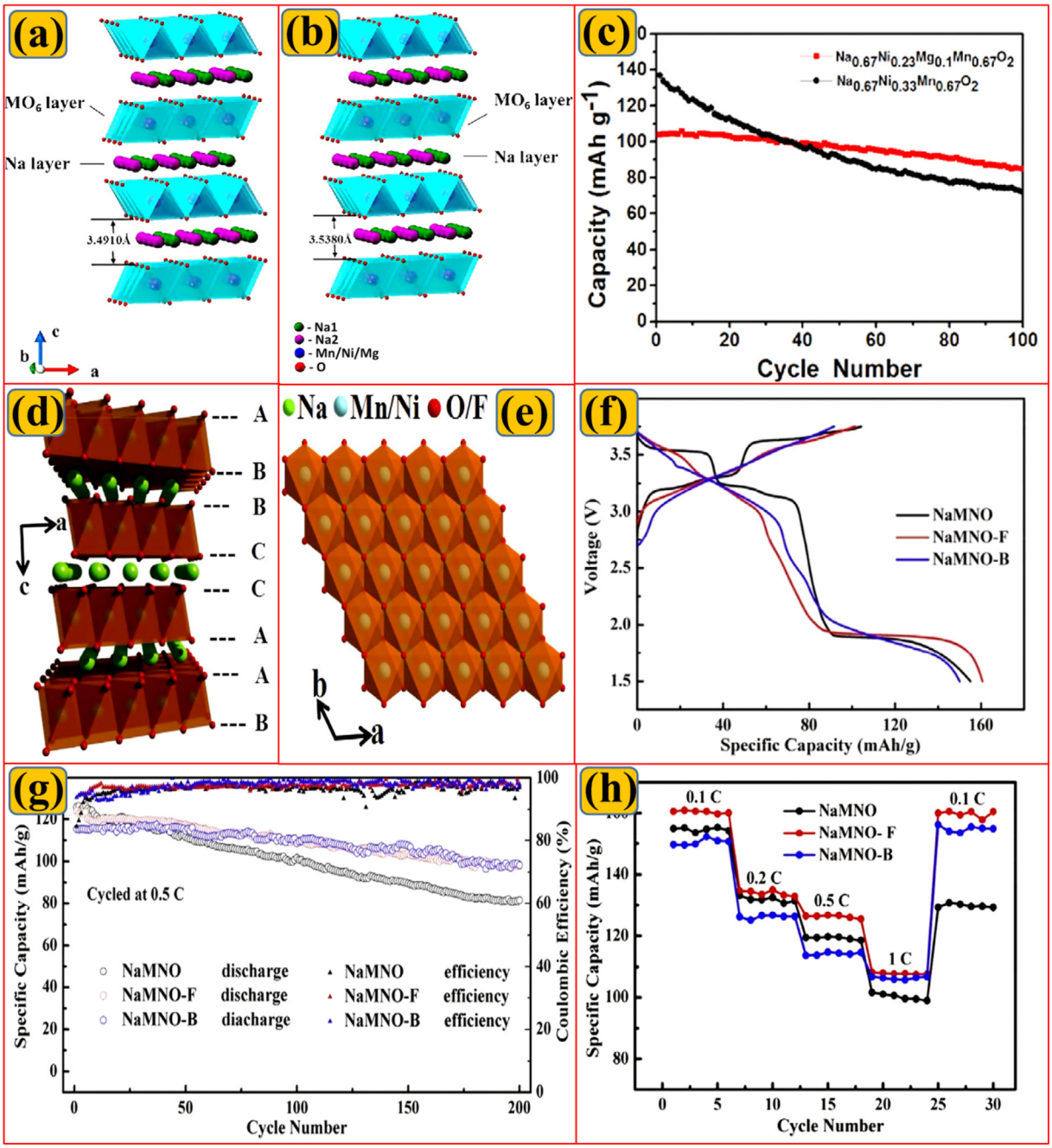


Fig. 5. (a) Crystal structure representation of $Na_{0.67}Mn_{0.67}Ni_{0.33}O_2$, (b) $Na_{0.67}Mg_{0.1}Ni_{0.23}Mn_{0.67}O_2$, (c) cyclic performance of $Na_{0.67}Mn_{0.67}Ni_{0.33}O_2$ and $Na_{0.67}Mg_{0.1}Ni_{0.23}Mn_{0.67}O_2$ at a current density of 48 mA g^{-1}. Reproduced with permission from Ref. [48]. Copyright 2016, American Chemical Society. (d) Crystal representation of P3-type along with *b* axis, (e) crystal representation of P3-type along with *c* axis, (f) the initial discharge and charge profiles, (g) cycling performance, and (h) rate performance of NaMNO, NaMNO-F, and NaMNO-B layered cathode material. Reproduced with permission from Ref. [41]. Copyright 2019, Elsevier.

the development of SIBs. First, F doping maintains a strong bond between TM and F and suppresses P3-O1 phase changes; thus, the F-doped cathode material exhibits good cycling performance during the cycling process. Second, B (boron)-B-doping stabilizes the structure and suppresses the oxidation and reduction of oxygen anions, and the cathode material can transition from the unstable P3 phase to a more reliable P2 phase. Accordingly, the B-doped cathode material exhibited a superior cycle life and rate performance. Thus, enhancing the electrochemical characteristics of layered cathode materials with the least amount of nonmetallic doping is a potential strategy. The initial discharge capacities of the layered NaMNO-B, NaMNO-F, and NaMNO cathode materials were 150, 163.7, and 156.3 mA h g^{-1} at a 0.1 current rate of 1.5 to 3.75 V. The layered NaMNO-B, NaMNO-F, and NaMNO electrodes provided the capacities of 115.7, 128, and 122.4 mA h g^{-1} with capacity fades of 0.085%, 0.13%, and 0.225% at 0.5 C after 200 cycles, respectively. In addition, the current density returned to 0.1 C following the increased rates, and the layered NaMNO-B and NaMNO-F cathode materials almost recovered the maximum capacity compared to NaMNO, as shown in Fig. 5(d–h). Hence, the F- and B-doped cathode materials improve the cycling stability, rate capability, and discharge capacity of SIBs.

It has been thoroughly demonstrated that, in Li-rich materials, fluorination can delay the decrease in transition metal valence,

reduce structural distortion, and prevent irreversible oxygen loss [109]. Zhang et al. [110] prepared a layered O3-type F-doped $NaMn_{1/3}Ni_{1/3}Fe_{1/3}O_{1.99}F_{0.01}$ cathode material for SIBs via a one-step solid-state reaction. F-doping regulates the ratio of $Mn^{3+}/^{4+}$ and the binding energy of oxygen; it can inhibit the Jahn-Teller effect, and a greater sodium ion diffusion rate can be obtained via F-doping. Accordingly, F doping improved the rate performance of the prepared cathode materials and increased their cycling and structural stability. In addition, F doping increased the ionic and electronic conductivities of the prepared materials.

A suitable cation or anion can be doped into the electrode to activate the redox activity of lattice oxygen, thereby increasing the electrode capacity. For instance, Mg doping creates strong ionic bonds with oxygen to increase the energy density of SIBs, initiate the oxygen redox reaction and provide charge compensation. According to the experimental results, the minimum quantity of elemental doping can help avoid phase changes, decrease the Jahn-Teller effect, diminish cation mixing, and enhance the ionic conductivity to improve the electrochemical performance of the layered materials. However, the effects of minor elements doped in layered cathode materials are complex, and further study in this area is required [111,112].

5.3. Structural design

Layered materials commonly have problems such as significant volume changes and poor ionic conductivity during the charge and discharge processes. The aforementioned issues can be resolved by modifying the size of the cathode materials, producing distinctive shapes, and developing hollow nano or micro structures. In general, spherical particles of uniform size are a good option for obtaining materials with greater tap density because they have a greater volume energy density than irregular particles. For example, Kaliyappan et al. [61] synthesized layered P2-type $Na_{0.66}(Ni_{0.13}Co_{0.13}Mn_{0.54})O_2$ (Na-NMC-180) spherical-shaped particles with a uniform size of 5 μm via the hydrothermal method heated at 180 °C as shown in Fig. 6(a–c). Ethylene, glycol, and urea were utilized to control the tap density, particle size, and particle shape of the prepared cathode materials, and the hydrothermal method was found to be more practical and convenient than the co-precipitation method. The Na-NMC-180 cathode material has a discharge capacity of 120 mA h g^{-1} at a 1 C rate, a voltage range of 2–4.7 V, and a sustained cycling durability of 90% after 150 cycles (Fig. 6d). The prepared cathode material exhibits superior electrochemical performances with a high tap density of 2.34 g cm^{-3} at the high voltage of 4.7 V. Because of the homogeneous size of the spherical particles, the layered cathode material has strong cyclability and a higher energy density; it also promotes sodium ion diffusion.

The anisotropic transition of the crystal lattice parameters occurred because of the frequent sodium-ion extraction/insertion of the cathode and the irreversible phase change during the electrochemical reaction. Consequently, considerable strain and microcracks are observed near the particle boundaries. Additionally, the constant contraction and expansion of the lattice minimizes the particle interaction. The rate capability and cycling durability of the cathode material are reduced for the aforementioned reasons. Single-crystal particles have good high-voltage stability compared with polycrystalline particles and provide a solution for intergranular cracks [113]. Su et al. [114] prepared a layered single crystalline $Na_{0.7}MnO_2$-nanoplate cathode material via the hydrothermal method. The $Na_{0.7}MnO_2$ single crystal was confirmed by high-resolution transmission electron microscopy (HR-TEM) and selected area electron diffraction (SAED), which revealed a 100-crystal plane (Fig. 6e–h). Consequently, sodium ion insertion and extraction were facilitated. The prepared cathode material had a high initial discharge capacity of 163 mA h g^{-1}. The $Na_{0.7}MnO_2$-nanoplate cathode material exhibited good cycling and structural stability and high rate performance after cycling.

Because of their significant sodium-ion storage sites and high specific surface area, hollow nano/micro structured materials have superior structural stability and high rate performance [115]. Mao et al. [116] reported layered $NaMn_{0.5}Ni_{0.5}O_2$ hollow microbar cathode materials prepared via a co-precipitation method for SIBs. The layered cathode material demonstrated excellent rate capability with capacity retention of 70% after 500 cycles, and the voltage decay was almost suppressed. Furthermore, Lu et al. [117] reported that hollow microspheres reduce the ion diffusion length and improve the contact area with the electrolyte. Volume change and ionic conductivity issues can be partially resolved using hollow micro/nanostructured materials. However, hollow nano/micro structured materials have a lower tap density than solid particles, resulting in a lower volume energy density. Thus, it is necessary to achieve an appropriate balance between the electrochemical properties and energy density.

Furthermore, the electrochemical performance, structural and cycling stability, vibration density, and rate capability of materials are mainly associated with the crystal structure, surface morphology, and particle size of the cathodes. Single-crystal structured materials improve the structural and cycling durability of cathode materials; however, there are some issues with the preparation of single-crystal structured materials, such as an irregular shape and size and particle aggregation. In addition, hollow nano/micro structured materials exhibit good electronic and ionic conductivities and high specific surface areas. However, they have some drawbacks, such as lower energy density and intensified side reactions.

5.4. Surface alteration

The performance of batteries degrades because of low ionic conductivity, side reactions between the electrode materials, a large volume strain, irreversible phase changes, and the dissolution of layered-structured cathode materials. To solve these problems, the electrical and ionic conductivities of cathode materials can be improved by surface treatment, which shields the active portion of the cathode materials from the effects of CO_2 and humidity. Furthermore, it reduces the side reactions of the electrolyte and electrode materials and the insulation that forms on the surface of the cathode material, such as Na_2CO_3 and NaOH [118–120].

In general, the performance of materials is significantly influenced by coating uniformity and thickness. The materials have lower ionic and electronic conductivities if the coating is uneven or thick. Atomic layer deposition (ALD) and molecular layer deposition (MLD) can be used to uniformly coat electrode surfaces with metal oxides. These techniques have been widely used to enhance the electrochemical properties of LIB and SIB cathodes. Ramasamy et al. [2] evaluated a layered Al_2O_3-coated P2-type $Na_{0.5}Mn_{0.5}Co_{0.5}O_2$ cathode material prepared via a polyol method using atomic layer deposition for SIBs. The Al_2O_3-coated cathode material exhibited a good rate performance and a high discharge capacity of 174 mA h g^{-1}. The formation of the cathode electrolyte interphase (CEI) layer on the surface was stabilized by surface modification (Al_2O_3 coating), which minimized electrolyte oxidation at higher voltages by lowering the charge transfer resistance. In addition, the durability and cell safety of layered cathode materials can be maintained through interfacial engineering, even at higher temperatures.

Kong et al. [121] synthesized layered P2-$Na_{0.67}Fe_{0.5}Mn_{0.5}O_2$ (MF) and MgO-coated P2-$Na_{0.67}Fe_{0.5}Mn_{0.5}O_2$ (MgO@MF) cathode materials for SIBs using the sol–gel technique. The MgO coating alleviated the transformation of the interlayer spacing and irreversible phase changes during cycling (Fig. 7a–c). The MgO coating

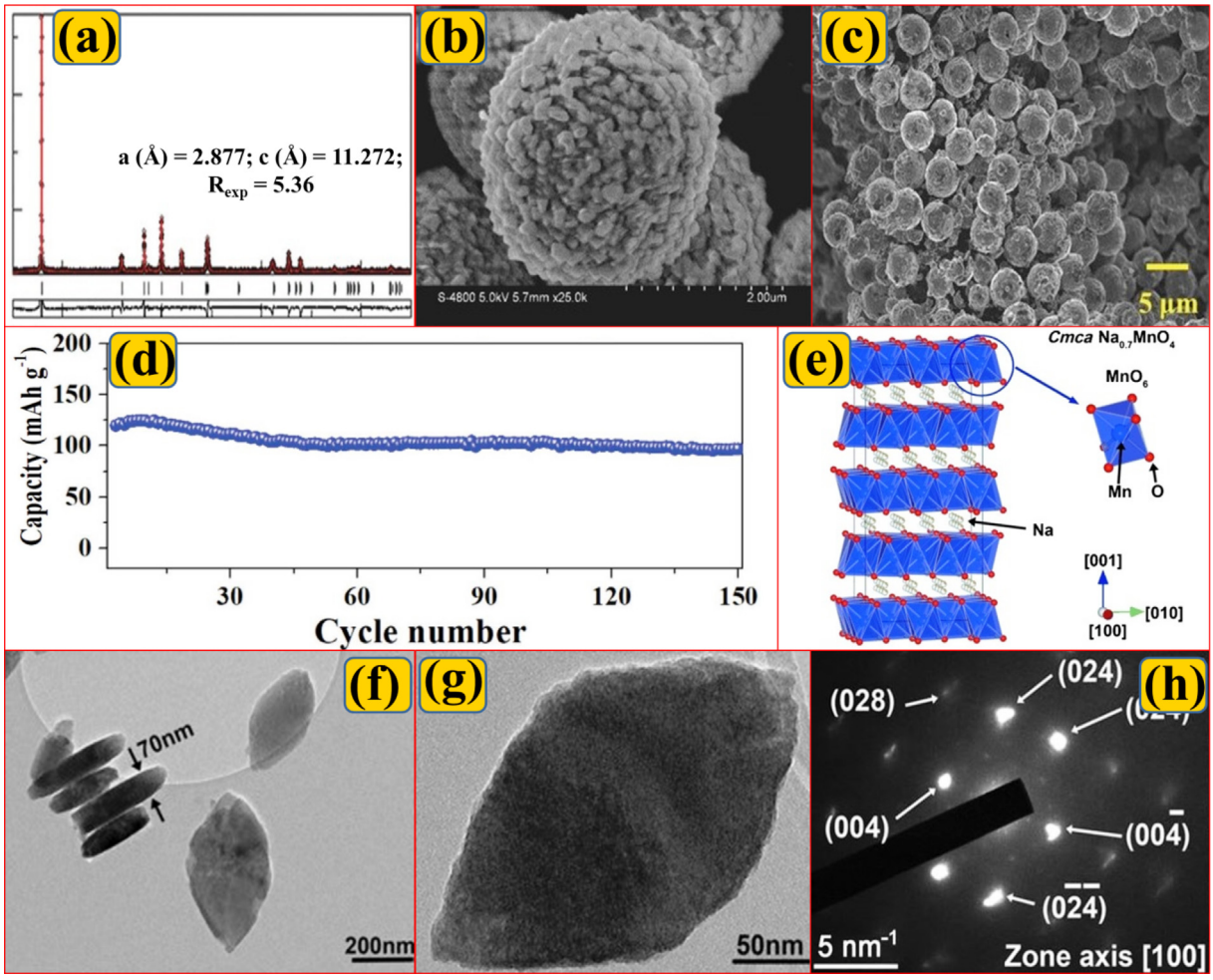


Fig. 6. (a) Rietveld refinement result, (b and c) SEM images of Na-NMC-180, (d) cyclic performance of NaNMC180. Reproduced with permission from Ref. [61]. Copyright 2018, Wiley-VCH. (e) Crystal representation of de-intercalated $Na_{0.7}MnO_2$ nanoplates, (f) a few free-standing $Na_{0.7}MnO_2$ nanoplates, (g) individual $Na_{0.7}MnO_2$ nanoplate TEM image, and (h) Tthe SAED pattern along the [100] zone axis of the $Na_{0.7}MnO_2$. Reproduced with permission from Ref. [114]. Copyright 2013, Wiley-VCH.

improved the ionic and electronic conductivities and reduced the interfacial resistance. Moreover, the MgO coating hindered transition metal ion dissolution and minimized side reactions between the electrode material surface and the electrolyte contact, which increased the structural stability of the materials. Besides, the capacity retention of the $Na_{0.67}Fe_{0.5}Mn_{0.5}O_2$ cathode materials ratio was increased from 20% to 70% at a 1 C rate after 100 cycles of MgO-coating and the rate capability of MgO@MF were obviously superior compared to bare MF, as shown in Fig. 7(d and e).

Zhang et al. [122] prepared layered $Na_{0.44}MnO_2$ and 2.5 wt%, 2 wt%, and 1 wt% Al_2O_3 coated $Na_{0.44}MnO_2$ single-crystal submicron rods via a conventional solid-state reaction for SIBs. The 110 mA h g^{-1} discharge capacity was obtained by the 2 wt% Al_2O_3 coated $Na_{0.44}MnO_2$ submicron rods at a 0.1 C rate in the voltage range between 2.0 and 4.5 V, and a capacity retention of 93% was maintained after 200 cycles (Fig. 7f–i). The Al_2O_3 coating effectively stabilized the $Na_{0.44}MnO_2$ submicron rod structure, protected the surface of the produced material from electrolyte contact, and inhibited volume expansion during cycling. After 500 cycles, the 2 wt% Al_2O_3 coated cathode material was maintained at 79% capacity retention in the long cycling performance with a current density of 4 C than pristine (45%). Therefore, it is clear that surface alteration significantly enhances the electrochemical performance of cathodes [123].

Moreover, small amounts of elemental doping and surface alteration have received considerable attention as effective and simple techniques for improving the properties of materials. Nonetheless, during electrochemical reactions, surface modification is commonly used to reduce side reactions between the surface of the electrode and the electrolyte; however, it cannot prevent structural volume changes and irreversible phase changes. Therefore, surface alteration and a minimum amount of elemental doping are typically utilized to improve the electrochemical characteristics of sodium-based layered cathode materials. Furthermore, the issues of poor electrochemical properties, irreversible phase changes, and instability of the cathode materials can be resolved using the elemental phase composition, a small amount of elemental doping, structural design, and surface alteration of the layered materials [124,125].

Besides, the thermal stability of the layered cathode materials, which has been examined by a diversity of methods for example differential scanning calorimetry, time-resolved X-ray diffraction, and accelerating rate calorimetry. Nonetheless, thermal safety related problems have not been effectively evaluated. Hwang et al. [126] investigated that the thermal stability of the P2-Na_xCoO_2 cathode material for SIBs using real-time transmission electron microscopy. The surface of Na_xCoO_2 became porous as the temperature increased due to the thermal decomposition to

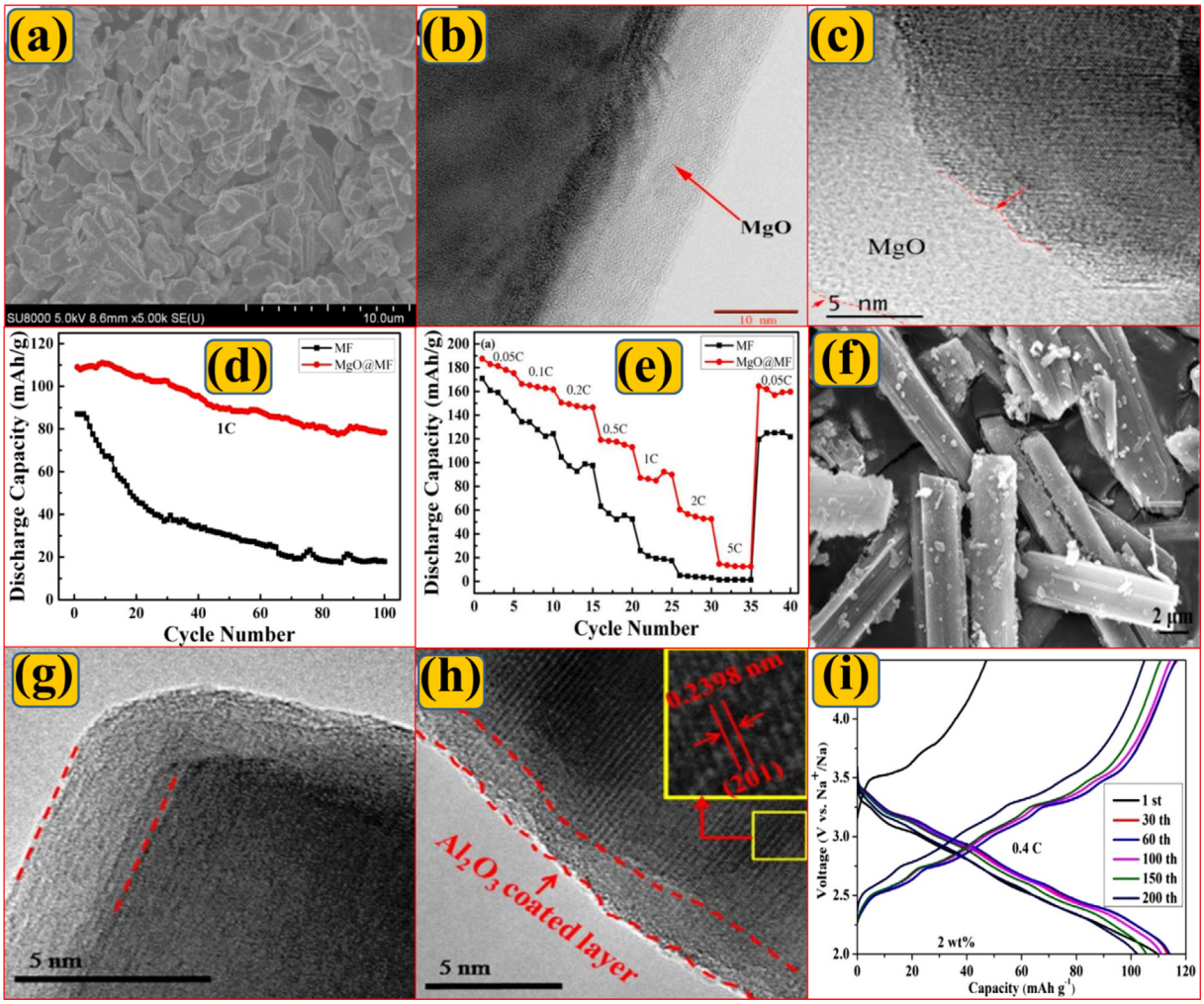


Fig. 7. (a) SEM image, (b and c) HR-TEM images of the MgO@MF material, (d) cycling behavior, (e) rate capability of the MgO@MF and MF materials at 1 C rate. Reproduced with permission from Ref. [121]. Copyright 2019, Elsevier. (f) SEM image, (g and h) HR-TEM images of Al_2O_3-coated (2 wt%) $Na_{0.44}MnO_2$ layered cathode material, and (i) the charge and discharge profile of Al_2O_3-coated (2 wt%) $Na_{0.44}MnO_2$ at 0.4 C rate. Reproduced with permission from Ref. [122]. Copyright 2019, Elsevier.

Co_3O_4, CoO, and Co with the reduction of Co. At the same temperature, larger cutoff voltages increased the degree of thermal decomposition. Significant changes in the morphology, as well as the crystallographic and electronic structures, were observed at the harshest conditions of 4.3 V cutoff voltage and 400 °C used in this investigation, as a result of the reduction of Co to the metallic state and the loss of oxygen, which are serious safety threats to the battery system's life. The electrode materials need to be thermally stable because SIBs are being developed for large-scale applications, which raise the risk of heat management failure and the negative effects of unwanted excessive heat. Hence, in order to increase thermal stability, the layered cathode materials should be improved. In order to prevent the thermal degradation of layered cathode materials for SIBs, techniques including surface coating, adding and optimizing transition metal compositions into the structure or controlling the crystal structure are thought to be beneficial.

6. Recent research progress on layered materials for SIBs

Many researchers have extensively evaluated the development of layered-type cathode materials for SIBs, especially layered structures such as unary, binary, ternary, quaternary, quinary, and senary-based O3- and P2-type cathode materials. Recent research progress on the aforementioned layered materials is described in detail below.

6.1. Unary, binary, ternary, quaternary, quinary, and senary-based O3-type cathodes

Lin et al. [127] prepared an oxygen-vacancy-enriched $NaCrO_{2-x}$ (OV-NCO) cathode material and a $NaCrO_2$ (S-NCO) cathode material via hydrogen reduction assisted by the spray drying method and the conventional solid-state method for SIBs, respectively. Ex-situ XRD and XPS demonstrate the exact process by which oxygen vacancies limit hazardous phase changes and store the majority of the overall capacity of O3-type exposed materials. The OV-NCO cathode material provides a capacity retention of 80.2% and a discharge capacity of 116.6 mA h g^{-1} at a 5 C rate after 400 cycles in the voltage range between 1.5 and 3.8 V. The S-NCO cathode material provides a capacity retention of 42.5% and a discharge capacity of 99.6 mA h g^{-1} after 400 cycles in the voltage range from 1.5 to 3.8 V at a 5 C rate. This suggests that the OV-NCO cathode exhibits superior cycling stability to that of S-NCO for high-rate SIBs. Jayachitra et al. [128] synthesized an activated carbon-coated O3-$NaFeO_2$ (Ac-coated NIO) cathode material for SIBs via a hydrothermal method. The carbon coating on the surface

alters the NIO surface, reduces the charge transfer resistance, improves the electron transport characteristics, and activates the SEI layer. Consequently, the electrochemical performance of the cathode material produced for SIBs was improved by the Ac-coated NIO. Alam et al. [60] synthesized fluorine (F) added O3-$NaFe_{0.5}Mg_{0.5}O_2$ cathode material through the hydrothermal method. The addition of fluorine stabilized the cathode material even at higher voltages and improved its electrochemical performance. For example, it offered a discharge capacity of 171.35 mA h g^{-1} at 50 mA g^{-1} with a capacity retention rate of 89% after 100 cycles in the voltage range of 2.0–4.5 V.

Xu et al. [129] prepared an O3-type layered $NaFe_{0.2}Ni_{0.3}Mn_{0.5}O_2$ cathode material for high-energy SIBs using a solid-phase method. Owing to the more stable transition metal oxide layer and the inhibition of the Jahn-Teller effect induced by Mn^{3+}, the layered O3-type cathode material had a capacity retention of 77% after 100 cycles and an initial discharge capacity of 139 mA h g^{-1} between 2 and 4.2 V at a 0.1 C rate. Furthermore, owing to its higher Na^+ diffusion rate and wider Na layer spacing, O3– $NaFe_{0.2}Ni_{0.3}Mn_{0.5}O_2$ has a discharge capacity of 116 mA h g^{-1} at 5 C. Therefore, the prepared layered O3-type cathode material is a potential candidate for commercial SIBs. Zhao et al. [130] synthesized a layered 2 wt% $NaTi_2(PO_4)_3$ coated O3-type $NaFe_{1/3}Ni_{1/3}Mn_{1/3}O_2$ (2 wt% NTP-coated NFM) cathode material using a co-precipitation method for high-rate SIBs. The electrolyte decomposition and solubility of redox-active metals were protected from hydrofluoric acid (HF) assault by the 2 wt% NTP coating. The movement of Na^+ ions may also have increased. In addition, Ti^{4+} was incorporated into the crystal structure, which enlarged the interlayer gap, improved the Na^+ diffusion coefficient, produced faster kinetics, and decreased the charge-transfer impedance. The 2 wt% NTP coated NFM cathode material significantly enhanced the cycling performance; for example, it exhibits a better rate capability and a capacity retention of 77.5% after 100 cycles at 0.1 C.

The layered O3-type $NaNi_{0.45}Mn_{0.4}Mg_{0.05}Ti_{0.1}O_2$ (NMMT) cathode material was successfully prepared via a classical solid-state reaction by Zhao et al. [131]. Mg and Ti co-doping in the TMO layers suppressed multiple phase transitions (O3-O'3-P3-P'3-O3′) and exhibited a single phase change (O3-P3). The NMMT cathode has a high discharge capacity of 86.6 mA h g^{-1} after 100 cycles in the voltage range of 2.0–4.5 V and a capacity retention of 82.3% after 200 cycles in the voltage range of 2–4 V at a 1 C rate. There are only a few examples of the outstanding cycling performance of NMMT cathodes. Co-doping can efficiently enhance the structural durability and integrity as well as the cycling performance of the prepared material for SIBs. Gogula et al. [132] prepared an O3-type $NaNi_{0.5}Ti_{0.3}Co_{0.1}Sb_{0.1}O_2$ cathode material for high-energy SIBs using a facile solid-state reaction. Various oxidation-state transition metals such as Ni, Ti, Co, and metalloid Sb in the layered composition lead to the creation of a cation-disordered structure, which improves the redox, structural durability, electronic conductivity, and working voltage. In addition, co-doping inhibited multiphase changes during electrochemical reactions. Therefore, the prepared O3-type cathode material enhanced the structural and cycling durability of SIBs.

Zhang et al. [133] synthesized a layered O3-type La-doped Na$(Ni_{0.4}Mn_{0.4}Cu_{0.1}Ti_{0.1})_{1-0.001}La_{0.001}O_2$ (NMCT-$La_{0.001}$) cathode material for SIBs using spray pyrolysis. The diffusion coefficient of sodium ions is increased by La-doping because it widens the interlayer space of the layered oxides. Owing to the higher bonding energy of La–O, La doping inhibits the Jahn-Teller effect induced by Mn^{3+}. After 30 days in the air and soaking in water, the NMCT-$La_{0.001}$ could still maintain its original composition and exhibited a reversible capacity of 129 mA h g^{-1}. In addition, a small amount of La substitution in the TMO layer improved the cycling and structural stability. Consequently, La doping provides a quick and effective way to develop high-rate cathode materials for SIBs. Tian et al. [134] prepared a high-entropy oxide six-component-layered O3-type $Na(Ni_{0.2}Ti_{0.2}Sn_{0.1}Li_{0.1}Fe_{0.2}Co_{0.2})O_2$ (NFCNTSL) cathode material for SIBs using a standard solid-state reaction. High-entropy oxides can efficiently inhibit phase transition, improve structural stability and provide excellent long-term durability. The improved electrochemical properties are caused by the disordered distribution of (multi-component) transition metals in the HEO, which inhibits the ordering of sodium vacancies and electric charges, thereby avoiding phase changes and interlayer movement.

High entropy oxides (HEOs) are a novel technique to develop advanced materials with unique features like traditional materials with only one or many dominant elements cannot attain. HEOs are multielement metallic systems that can crystallize in a single phase, with distinct systems having various crystal forms, such as spinel, single-phase rock-salt, and perovskite structures. In general, five or more main elements share the equiatomic positions in HEO, which can stabilize the solid-solution state. Because of their exceedingly complex composition, these materials frequently reveal excellent performances like high strength, high fracture toughness, worthy energy storage properties, and good high/low temperature performance, etc. For example, the HEO material, such as the layered cathode O3-type $NaNi_{0.12}Co_{0.15}Cu_{0.12}Fe_{0.15}Sn_{0.1}Mg_{0.12}Mn_{0.1}Sb_{0.04}Ti_{0.1}O_2$ (NMCFCMSTS) material, was effectively prepared via the traditional solid-state reaction by Zhao et al. [135] for SIBs. The NMCFCMSTS cathode material has a better rate capability with a capacity retention of 80% at a 5 C rate and long-term cyclability at various C rates; for example, a capacity retention of 83% in the voltage range of 2–3.9 V after 500 cycles. Moreover, in the O3-type domain, which displays a highly reversible O3-P3 phase-transition behavior, more than 60% of the total capacity can be observed. Besides, The HEO of the NMCFCMSTS cathode material provides a discharge capacity of 110 mA h g^{-1} with a greater rate capability and long-term cycle stability. According to the above mentioned results, the high-entropy chemistry will open new opportunities to tailor advanced layered structured cathode materials.

Moreover, Peng et al. [136] synthesized a layered O3-type $NaNi_{0.5}Mn_{0.5}O_2$ (NNMO) and Al-doped O3-$NaNi_{0.45}Al_{0.1}Mn_{0.45}O_2$ (O3-NNAMO) cathode materials for SIBs using traditional sol–gel method (Fig. 8a–e). When a small amount of Aluminum (Al) is doped, the TMO_2 layer decreases and the Na layer increases, showing that Al doping considerably changes the local chemical environment. Hence, the sodium ions easily migrated during the electrochemical reaction. The effect of local chemical environment regulation is confirmed simultaneously to inhibit the complicated phase transitions and decrease the sodium ions diffusion energy barrier, which are the reason for the impressive enhanced electrochemical performances of the cathode materials. Besides, the TEM image confirms that the O3-NNAMO material is composed of irregular nanoparticles. The O3-NNAMO cathode has a high discharge capacity of 104 mA h g^{-1} and capacity retention of 82.6% after 100 cycles with good rate performance in the voltage range of 2–4 V at a 0.1 C rate. Therefore, Al-doping can efficiently enhance the structural durability and integrity as well as the cycling performance of the prepared material for SIBs. Furthermore, the recent research overview of methods and electrochemical performances of the layered O3-type unary, binary, ternary, quaternary, quinary, and senary based cathode materials are listed in Table S1.

6.2. Unary, binary, ternary, quaternary, quinary, and senary-based P2-type cathodes

The layered P2-$NaCoO_2$ cathode material was effectively synthesized via sol–gel for high-rate SIBs by Boddu et al. [137]. The well-ordered highly crystalline layered P2-$NaCoO_2$ structure was

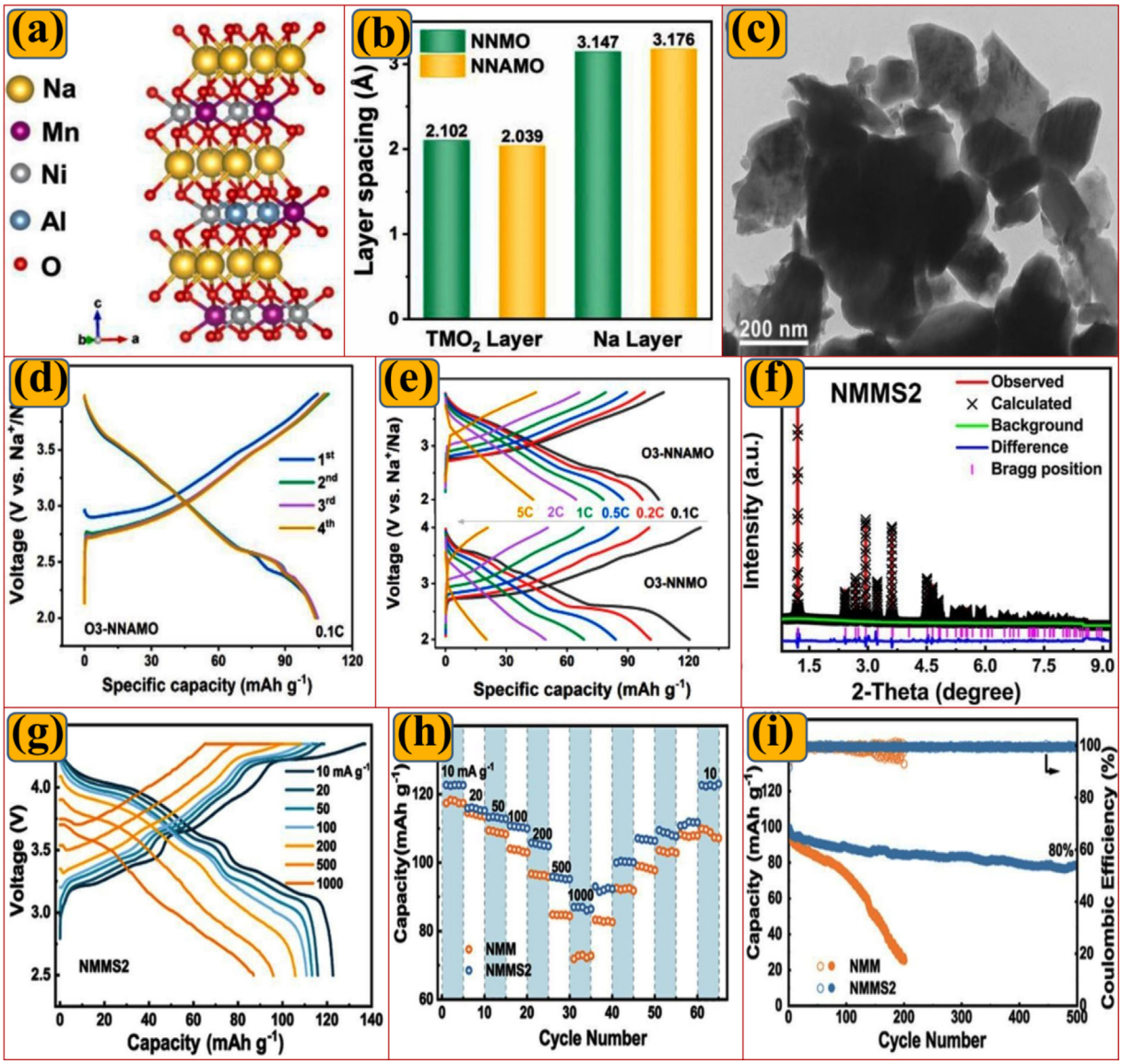


Fig. 8. (a) Crystal representation of O3-NNAMO, (b) TMO_2 and Na layer spacing of O3-NNMO and O3-NNAMO, (c) TEM image of O3-NNAMO, (d) charge and discharge profile of O3-NNAMO, (e) rate performances of the O3-NNMO and O3-NNAMO cathode materials. Reproduced with permission from Ref. [136]. Copyright 2023, Elsevier. (f) Rietveld plot of NMMS2, (g) charge and discharge profile of NMMS2 at different current densities between 2.5–4.35 V, (h) rate cycling performance and corresponding midpoint discharge voltage, and (i) specific capacity with coulombic efficiency at 500 mA g^{-1} of NMM and NMMS2. Reproduced with permission from Ref. [147]. Copyright 2023, American Chemical Society.

obtained and optimized the condition at 750 °C for 28 h using high-temperature furnace without any impurities, which can improves the sodium ion storage capacity. According to the condition, it revealed excellent electrochemical performance at different current densities for SIBs. Wen et al. [138] prepared titanium (Ti) and fluorine (F) doped P2-type P2-$Na_{0.7}MnO_{2.05}$ cathode material for long life and high capacity SIBs using typical solid-state reaction. Ti and F co-doping considerably inhibits the irreversible phase transitions, improves the electrochemical kinetics, decreases the structural deformation, and enhances the structural stabilization. High discharge capacity of 227 mA h g^{-1} in the voltage range of 2–4.2 V at 20 mA g^{-1}, improved rate capability, and long-term cycling durability with capacity retention of 96.2% at 1 A g^{-1} after 200 cycles is all provided by the co-doped layered P2-$Na_{0.7}MnO_{2.05}$ cathode. Therefore, high capacity and stable P2-$Na_{0.7}MnO_{2.05}$ cathode material is auspicious solution for practical SIBs applications.

Kim et al. [139] synthesized layered P2-$Na_{0.67}Cu_{0.33}Mn_{0.67}O_2$ cathode for emerging SIBs using spray pyrolysis method. The high crystalline layered $Na_{0.67}Cu_{0.33}Mn_{0.67}O_2$ structure was obtained and optimized the condition at 750 °C for 10 h; it can increase the sodium ion storage capacity. The fast sodium ions transport kinetics of $Na_{0.67}Cu_{0.33}Mn_{0.67}O_2$ led to good rate capabilities and stable cycling performance for Na^+ storage properties and during electrochemical reaction, no phase changes were observed. Furthermore, the layered P2-type carbon coated cathode $NaMn_{0.8}Li_{0.2}O_2$ material was effectively prepared via classical SSR for SIBs by Quyen et al. [140]. The carbon coating has decreased the resistance and modified the surface of the $NaMn_{0.8}Li_{0.2}O_2$ cathode material, which improves the cycling performance, capacity, coulombic efficiency, and rate capability. Hence, carbon coated P2-type $NaMn_{0.8}Li_{0.2}O_2$ cathode material enhances electrochemical performance during cycling process for SIBs.

Zhang et al. [141] synthesized the single crystal hexagonal prism like P2-$N_{a0.66}$ $Zn_{0.07}Ni_{0.26}Mn_{0.67}O_2$ (MC-NNZM) layered cathode material for SIBs using combined co-precipitation and molten-salt method. The effective TMO_2 slab gliding suppression, which

results in a significant reduction in the volume change of MC-NNZM during electrochemical reaction, is shown to be the cause of the good electrochemical properties of MC-NNZM at high voltage. Thus, irreversible intergranular cracking and dislocations caused by mechanical stress can be significantly decreased in MC-NNZM, in contrast to the layered oxides composed of randomly oriented crystal planes. Additionally, the cathode has superior ionic/electronic transport performance because the robust single-crystal structure inhibits the continual accumulation of resistive side-products on the material surface caused on by electrolyte dissolution. In addition, the MC-NNZM provides a discharge capacity of 122.1 mA h g^{-1} with the capacity retention of 95.8% after 100 cycles at 10 mA g^{-1}. Therefore, the P2-type layered oxides electrochemical performance will be further enhanced by single-crystal particle size at high voltage. Deng et al. [142] synthesized the layered P2-type Co (cobalt)-doped and $Al_{1.8}Co_{0.2}O_3$ coated $Na_{0.67}Mn_{0.67}Ni_{0.33}O_2$ cathode material for SIBs using co-precipitation method. The Co-doping increases the rate capabilities but decreases the initial discharge capacity. Besides, the $Al_{1.8}Co_{0.2}O_3$ coatings hinder the interfacial side reactions and sustain the structural integrity of the cathode. The capacity retention of the layered Co-doped and $Al_{1.8}Co_{0.2}O_3$ coated $Na_{0.67}Mn_{0.67}Ni_{0.33}O_2$ (84.8%) is increased than pristine (65.8%).

The layered P2-type Cu and Li dual doped $Na_{0.93}Cu_{0.07}Li_{0.07}Mn_{0.57}Ni_{0.29}O_2$ (NLCMO-2) cathode was successfully synthesized through sol–gel method (citric acid assisted) for high energy SIBs by Anilkumar et al. [143]. The Cu and Li co-doping improves the electrochemical performances compared to pristine. By suppressing the P2-O2 phase transition, doping of Li and Cu acts as a structural support to stabilize the structure, increase the capacity at high voltage, and improve the sodium content. The co-doped P2-type cathode provides better discharge capacity of (110 mA h g^{-1}) with the capacity retention (85%) at 0.2 C rate after 200 cycles than pristine. Hence, co-doping in the TM site provides a cost-effective, stable, and high-performance cathode material for SIBs.

Furthermore, Ouyang et al. [144] synthesized layered K^+ (potassium) doped P2-$Na_{0.67}Mn_{0.6}Cu_{0.1}Ni_{0.3}O_2$ cathode for high rate SIBs using sol–gel method. In order to accommodate more sodium ions and produce rapid ion transport channels, the greater atomic radius of potassium ions occupies the sodium ions sites and enlarges the interlayer space. Besides, the increased layer gap generated by K^+ doping correlates to multiple-layer oriented stacking nanoflakes, which is extremely favorable for sodium ion transport. The K^+ doped cathode material displays excellent rate capabilities and cycling durability for instance, it have the capacity retention (92.8%) after 100th cycles at 0.1 C rate than pristine. Additionally, K^+ doped layered P2-type cathode material enhances stability of the materials when exposed to air and water conditions and also serves as a fortunate solution for promising SIBs.

The layered Ca (calcium) and Mg (magnesium) substituted P2-type cathode material $Na_{0.64}Ca_{0.03}(Mn_{0.66}Ni_{0.17}Co_{0.17})_{0.9}Mg_{0.1}O_2$ was successfully synthesized via co-precipitation method for SIBs by Su et al. [145]. The Mg substitution enhances the structural integrity of the P2-type cathode by preventing P2-O2 changes during charge and discharge. Besides, the Minimum quantity of Ca-doping in TMO sites enlarges the lattice spacing and increase the reversible capacity of electrode. Consequently, it reveals that the Ca and Mg co-doping can improve the cycle stability and rate capability of $Na_{0.67}Ni_{0.17}Co_{0.17}Mn_{0.66}O_2$ for SIBs. Moreover, Fu et al. [146] prepared multicomponent P2-type layered $Na_{2/3}Ni_{0.22}Mn_{0.67}Ti_{0.02}Al_{0.02}Cu_{0.05}O_2$ (NaNMTAlC) cathode material for SIBs. The small amount of Al (aluminum) substitution in TMO site decrease Jahn-Teller distortion. The small amount of Cu (copper) substitution in TMO site provide new redox center. The small amount of Ti (titanium) substitution in TMO site expands the interlayer distance. The NaNMTAlC P2-type material has outstanding high-rate performance and ultra-long cycling stability; for example, after 900 cycles at 10 C rate, it has a reversible capacity of 66 mA h g^{-1}. Hence, Al, Cu, and Ti substituted layered P2-type cathode material is suitable for high performances SIBs. Additionally, the layered P2-$Na_{0.67}Ni_{0.23}Mg_{0.1}Mn_{0.67}O_2$ (NMM) and P2-$Na_{0.67}Ni_{0.23}Mg_{0.1}Sn_{0.02}Mn_{0.65}O_2$ (NMMS2) cathode materials were successfully prepared via a classical solid-state reaction by Yuan et al. [147]. The P2-NMMS2 material delivered the discharge capacity 110 mA h g^{-1} and capacity retention of 80% after 500 cycles. After the high rate cycles, the current density returned to 10 mA g^{-1} and the NMMS2 restored maximum capacity, implying that the NMMS2 cathode improved the sodium ion transport kinetics (Fig. 8f–i). Besides, Mg and Sn co-substitution in TMO layer considerably improve moisture stability, Na^+ diffusion, and structural reversibility. Due to robust TMO_2 slabs with expanded lattice spacing and strong SnO bonds, the P2-NMMS2 cathode demonstrated outstanding rate capability and cyclic stability. Therefore, the prepared layered P2-NMMS2 cathode material is a potential candidate for commercial SIBs.

Furthermore, recently, the layered structured P2-type $Na_{0.67}(Mn_{0.55}Co_{0.24}Ni_{0.21})O_2$ (low-entropy), $Na_{0.67}(Mn_{0.45}Ti_{0.1}Ni_{0.18}Co_{0.24}Mg_{0.03})O_2$ (medium-entropy), and $Na_{0.67}(Mn_{0.45}Ti_{0.1}Ni_{0.18}Co_{0.18}Mg_{0.03}Al_{0.04}Fe_{0.02})O_2$ (high-entropy) cathode materials were effectively synthesized through a traditional solid-state reaction for SIBs by Wang et al. [148]. In the potential ranges of 2.6–4.6 V and 1.5–4.6 V, it was discovered that the high-entropy cathode material exhibited superior reversibility during cycling. Conversely, in the case of low-entropy, rapid capacity fading was observed and moderate capacity decay for medium-entropy. Combining ex-situ XRD and operando, it was found that after many cycles, all materials tend to undergo a solid-solution reaction, accompanied by a weakening of the P2 → O2 phase transition. The high entropy cathode material serves to mitigate phase transition and sustain structural stability compared to low and medium-entropy. Overall, the high-entropy approach is an auspicious way for enhancing electrochemical properties of the P2-type layered cathode materials for practical SIB applications. Moreover, the recent research overview of methods and electrochemical performances of the layered P2-type unary, binary, ternary, quaternary, quinary, and senary based cathode materials are listed in Table S2. According to the above mentioned results, the small amount of transition metal substitution in TMO layer improved cycling and structural stability of the O3 and P2-type layered cathode materials during electrochemical reaction by suppressing phase transition, increasing ionic conductivity, and decreasing Jahn-Teller distortion. Therefore, minimum quantity of TMO substituted layered O3 and P2-type cathode materials are promising solution for SIBs systems.

Finally, the layered O3 and P2-type transition metal oxide cathode materials exhibits high specific capacity, outstanding rate capability, and worthy structural and cycling stability. Besides, O3 and P2-type layered cathode materials have the benefits of easy synthesis process, plentiful and low-cost raw materials, non-toxic, and ecological friendly for SIBs. However, additional optimization of their energy density, cycle life, coulombic efficiency, and air stability is still required for practical applications.

7. Conclusion and perspectives

The research on layered Na transition metal oxide cathode materials for SIBs was extensively discussed in this review article.

The structural classification, material preparation, difficulties, and strategies for O3 and P2-type cathode materials were discussed. The main problems with layered O3 and P2-type cathode materials include numerous phase changes, poor air stability, and poor electrochemical performance during electrochemical reactions. Moreover, many appropriate tactics have been designed to solve the above-mentioned problems, for example, modification of elemental phase composition (the mixed prismatic and octahedral biphasic phase), small amounts of elemental doping (Ti, Mg, Al, Zn, Cu, F, and Li), structural design (hollow nano or micro structures), and surface alteration (AL_2O_3 coating and MgO coating). Furthermore, the current research progress on layered unary, binary, ternary, quaternary, quinary, and senary-based O3 and P2-type cathode materials for SIBs was systematically evaluated.

Nevertheless, many factors must be addressed, particularly in terms of cost-effectiveness. The enhancement of the energy density should be the primary goal of future research on layered sodium transition metal oxide cathode materials for SIBs, offering a steady sodium storage performance over a higher voltage range and greater specific capacity via oxygen redox reactions. Researchers across the world are constantly evaluating the best methods for manufacturing novel materials to produce batteries with low cost, long cycle life, and high energy density. Further optimization is required for other components in battery systems, including the electrolyte, separator, and anode. Although there are still many obstacles to overcome, we believe that layer-structured cathode materials may be useful in promoting the widespread use of inexpensive SIBs for large-scale energy storage applications in the near future.

Declaration of competing interest

The authors declare that they have no known competing financial interests or personal relationships that could have appeared to influence the work reported in this paper.

Acknowledgments

This work was supported by a grant from the Subway Fine Dust Reduction Technology Development Project of the Ministry of Land Infrastructure and Transport, Republic of Korea (21QPPW-B152306-03) and the Basic Science Research Capacity Enhancement Project through a Korea Basic Science Institute (National Research Facilities and Equipment Center) grant funded by the Ministry of Education of the Republic of Korea (2019R1A6C1010016).

Appendix A. Supplementary material

Supplementary data to this article can be found online at https://doi.org/10.1016/j.jechem.2023.10.023.

References

[1] Q. Liu, Z. Hu, M. Chen, C. Zou, H. Jin, S. Wang, S.L. Chou, S.X. Dou, Small 15 (2019) 1805381.
[2] H.V. Ramasamy, P.N. Didwal, S. Sinha, V. Aravindan, J. Heo, C.J. Park, Y.S. Lee, J. Colloid Interface Sci. 564 (2020) 467–477.
[3] H. Chen, P. Lv, P. Tian, S. Cao, S. Yuan, Q. Liu, J. Energy Chem. 82 (2023) 248–258.
[4] A. Zhao, Y. Fang, X. Ai, H. Yang, Y. Cao, J. Energy Chem. 60 (2021) 635–648.
[5] T.Y. Yu, J.Y. Hwang, I.T. Bae, H.G. Jung, Y.K. Sun, J. Power Sources 422 (2019) 1–8.
[6] S. Chu, Y. Chen, J. Wang, J. Dai, K. Liao, W. Zhou, Z. Shao, J. Alloy. Compd. 775 (2019) 383–392.
[7] J. Sun, Y. Sun, J.A.S. Oh, Q. Gu, W. Zheng, M. Goh, K. Zeng, Y. Cheng, L. Lu, J. Energy Chem. 62 (2021) 497–504.
[8] C. Senthil, J.W. Park, N. Shaji, G.S. Sim, C.W. Lee, J. Energy Chem. 64 (2022) 286–295.
[9] Y.M. Zheng, X.B. Huang, X.M. Meng, S.D. Xu, L. Chen, S.B. Liu, D. Zhang, ACS Appl. Mater. Interfaces 13 (2021) 45528–45537.
[10] Y. Wang, W. Li, G. Hu, Z. Peng, Y. Cao, H. Gao, K. Du, J.B. Goodenough, Chem. Mater. 31 (2019) 5214–5223.
[11] X. Yin, Y. Ren, L. Wu, Z. Zhang, C. Du, J. Wang, G. Yin, H. Huo, J. Energy Chem. 71 (2022) 210–217.
[12] S.H. Gong, J.H. Lee, D.W. Chun, J.H. Bae, S.C. Kim, S. Yu, S. Nahm, H.S. Kim, J. Energy Chem. 59 (2021) 465–472.
[13] J. Wang, X. He, D. Zhou, F. Schappacher, X. Zhang, H. Liu, M.C. Stan, X. Cao, R. Kloepsch, M.S. Sofy, G. Schumacher, J. Mater. Chem. A 4 (2016) 3431–3437.
[14] Y. Xiao, N.M. Abbasi, Y.F. Zhu, S. Li, S.J. Tan, W. Ling, L. Peng, T. Yang, L. Wang, X.D. Guo, Y.X. Yin, Adv. Funct. Mater. 30 (2020) 2001334.
[15] C. Hakim, N. Sabi, I. Saadoune, J. Energy Chem. 61 (2021) 47–60.
[16] L.J. Xie, C. Tang, M.X. Song, X.Q. Guo, X.M. Li, J.X. Li, C. Yan, Q.Q. Kong, G.H. Sun, Q. Zhang, F.Y. Su, J. Energy Chem. 72 (2022) 554–569.
[17] C. Wang, N. Cheng, Z. Bai, Q. Gu, F. Niu, X. Xu, J. Zhang, N. Wang, B. Ge, J. Yang, Y. Qian, J. Energy Chem. 77 (2023) 369–375.
[18] A.K. Prajapati, A. Bhatnagar, J. Energy Chem. 83 (2023) 509–540.
[19] G. Yao, X. Zhang, Y. Yan, J. Zhang, K. Song, J. Shi, L. Mi, J. Zheng, X. Feng, W. Chen, J. Energy Chem. 50 (2020) 387–394.
[20] J. Qian, C. Wu, Y. Cao, Z. Ma, Y. Huang, X. Ai, H. Yang, Adv. Energy Mater. 8 (2018) 1702619.
[21] M. Chen, L. Chen, Z. Hu, Q. Liu, B. Zhang, Y. Hu, Q. Gu, J.L. Wang, L.Z. Wang, X. Guo, S.L. Chou, Adv. Mater. 29 (2017) 1605535.
[22] S.P. Guo, J.C. Li, Q.T. Xu, Z. Ma, H.G. Xue, J. Power Sources 361 (2017) 285–299.
[23] R. Liu, Z. Liang, Z. Gong, Y. Yang, Small Methods. 3 (2019) 1800221.
[24] P.F. Wang, Y.J. Guo, H. Duan, T.T. Zuo, E. Hu, K. Attenkofer, H. Li, X.S. Zhao, Y.X. Yin, X. Yu, Y.G. Guo, ACS Energy Lett. 2 (2017) 2715–2722.
[25] K. Wang, H. Wan, P. Yan, X. Chen, J. Fu, Z. Liu, H. Deng, F. Gao, M. Sui, Adv. Mater. 31 (2019) 1904816.
[26] F. Wei, Q. Zhang, P. Zhang, W. Tian, K. Dai, L. Zhang, J. Mao, G. Shao, J. Electrochem. Soc. 168 (2021) 050524.
[27] Q. Liu, Z. Hu, W. Li, C. Zou, H. Jin, S. Wang, S. Chou, S.X. Dou, Energ. Environ. Sci. 14 (2021) 158–179.
[28] M. Sathiya, Q. Jacquet, M.L. Doublet, O.M. Karakulina, J. Hadermann, J.M. Tarascon, Adv. Energy Mater. 8 (2018) 1702599.
[29] Y. Singh, R. Parmar, S. Rani, M. Kumar, K.K. Maurya, V.N. Singh, Heliyon (2022) 10013.
[30] C. Zhang, R. Gao, L. Zheng, Y. Hao, X. Liu, ACS Appl. Mater. Interfaces 10 (2018) 10819–10827.
[31] R.M. Gao, Z.J. Zheng, P.F. Wang, C.Y. Wang, H. Ye, F.F. Cao, Energy Stor. Mater. 30 (2020) 9–26.
[32] A. Mauger, C.M. Julien, Materials 13 (2020) 3453.
[33] S. Guo, J. Yi, Y. Sun, H. Zhou, Energ. Environ. Sci. (2016) 2978–3006.
[34] N. Yabuuchi, K. Kubota, M. Dahbi, S. Komaba, Chem. Rev. 114 (2014) 11636–11682.
[35] J.Y. Hwang, S.T. Myung, Y.K. Sun, Chem. Soc. Rev. 46 (2017) 3529–3614.
[36] J.L. Yue, Y.N. Zhou, X. Yu, S.M. Bak, X.Q. Yang, Z.W. Fu, J. Mater. Chem. A 3 (2015) 23261–23267.
[37] J.Y. Hwang, J. Kim, T.Y. Yu, Y.K. Sun, Adv. Energy Mater. 9 (2019) 1803346.
[38] A. Kanwade, S. Gupta, A. Kankane, M.K. Tiwari, A. Srivastava, J.A.K. Satrughna, S.C. Yadav, P.M. Shirage, RSC Adv. 12 (2022) 23284–23310.
[39] Y. Fang, L. Xiao, Z. Chen, X. Ai, Y. Cao, H. Yang, Electrochemical Energy Reviews 1 (2018) 294–323.
[40] E.J. Kim, L.A. Ma, L.C. Duda, D.M. Pickup, A.V. Chadwick, R. Younesi, J.T. Irvine, A.R. Armstrong, ACS Appl. Energy Mater. 3 (2019) 184–191.
[41] Y. Wang, X. Wang, X. Li, R. Yu, M. Chen, K. Tang, X. Zhang, Chem. Eng. J. 360 (2019) 139–147.
[42] Y. Wang, K. Tang, X. Li, R. Yu, X. Zhang, Y. Huang, G. Chen, S. Jamil, S. Cao, X. Xie, Z. Luo, Chem. Eng. J. 372 (2019) 1066–1076.
[43] Y.N. Zhou, P.F. Wang, X.D. Zhang, L.B. Huang, W.P. Wang, Y.X. Yin, S. Xu, Y.G. Guo, ACS Appl. Mater. Interfaces 11 (2019) 24184–24191.
[44] T. Risthaus, L. Chen, J. Wang, J. Li, D. Zhou, L. Zhang, D. Ning, X. Cao, X. Zhang, G. Schumacher, M. Winter, Chem. Mater. 31 (2019) 5376–5383.
[45] M. Leng, J. Bi, W. Wang, R. Liu, C. Xia, Ionics 25 (2019) 1105–1115.
[46] G. Hu, Y. Liu, W. Li, Z. Peng, J. Wu, Z. Xue, Y. Shi, J. Fan, Q. Sun, Y. Cao, K. Du, Ionics 27 (2021) 657–666.
[47] Z.Y. Li, R. Gao, J. Zhang, X. Zhang, Z. Hu, X. Liu, J. Mater. Chem. A 4 (2016) 3453–3461.
[48] H. Hou, B. Gan, Y. Gong, N. Chen, C. Sun, Inorg. Chem. 55 (2016) 9033–9037.
[49] J. Zhang, H. Yuan, Z. Yang, Y. Huang, S. Kan, Y. Wu, P. He, H. Liu, Ind. & Eng. Chem. 58 (2019) 22804–22810.
[50] L. Wang, Y.G. Sun, L.L. Hu, J.Y. Piao, J. Guo, A. Manthiram, J. Ma, A.M. Cao, J. Mater. Chem. A 5 (2017) 8752–8761.
[51] F. Fiévet, S. Ammar-Merah, R. Brayner, F. Chau, M. Giraud, F. Mammeri, J. Peron, J.Y. Piquemal, L. Sicard, G. Viau, Chem. Soc. Rev. 47 (2018) 5187–5233.
[52] R. Muruganantham, M. Sivakumar, R. Subadevi, N.L. Wu, J. Mater. Sci. Mater. Electron. 26 (2015) 2095–2106.

[53] R. Muruganantham, M. Sivakumar, R. Subadevi, Ionics 24 (2018) 989–999.
[54] W. Kang, D.Y. Yu, P.K. Lee, Z. Zhang, H. Bian, W. Li, T.W. Ng, W. Zhang, C.S. Lee, ACS Appl. Mater. Interfaces 8 (2016) 31661–31668.
[55] N.A. Nguyen, K. Kim, K.H. Choi, H. Jeon, K. Lee, M.H. Ryou, Y.M. Lee, J. Electrochem. Soc. 164 (2016) A6308.
[56] Y. Wen, B. Wang, G. Zeng, K. Nogita, D. Ye, L. Wang, Chem. Asian J. 10 (2015) 661–666.
[57] Z. Zhang, Y. Meng, Y. Wang, H. Yuan, D. Xiao, ChemElectroChem 5 (2018) 3229–3235.
[58] C. Cheng Fu, J. Wang, Y. Li, G. Liu, T. Deng, J. Alloy. Compd. 918 (2022) 165569.
[59] D. Meghnani, R.K. Singh, Electrochim. Acta 419 (2022) 140403.
[60] M.W. Alam, A. BaQais, I. Nahvi, A. Yasin, T.A. Mir, S. Shajahan, Inorganics 11 (2023) 37.
[61] K. Kaliyappan, W. Xaio, T.K. Sham, X. Sun, Adv. Funct. Mater. 28 (2018) 1801898.
[62] A.S. Deepi, G. Srikesh, A.S. Nesaraj, Matéria (2021) 26.
[63] G. Savithiri, V. Priyanka, R. Subadevi, B.K. Das, M. Sivakumar, J. Taiwan Inst. Chem. Eng. 126 (2021) 197–204.
[64] G. Savithiri, V. Priyanka, R. Subadevi, M. Sivakumar, J. Nanopart. Res. 22 (2020) 1–11.
[65] W. Zhao, S. Harada, Y. Furuya, S. Yamamoto, H. Noguchi, J. Power Sources 261 (2014) 324–331.
[66] S.T. Aruna, Concise encyclopedia of self-propagating high-temperature synthesis (2017) 344–346.
[67] F.P. Nkosi, K. Raju, N. Palaniyandy, M.V. Reddy, C. Billing, K.I. Ozoemena, J. Electrochem. Soc. 164 (2017) A3362.
[68] M. Nanthagopal, C.W. Ho, N. Shaji, G.S. Sim, M. Varun Karthik, H.K. Kim, C.W. Lee, Nanomaterials 12 (2022) 984.
[69] V.K. Kumar, S. Ghosh, S. Ghosh, P.S. Behera, S. Biswas, S.K. Martha, J. Alloy. Compd. 924 (2022) 166444.
[70] V.S. Rangasamy, S. Thayumanasundaram, J.P. Locquet, Electrochim. Acta 276 (2018) 102–110.
[71] W. Li, Z. Yao, S. Zhang, X. Wang, X. Xia, C. Gu, J. Tu, Chem. Eng. J. 421 (2021) 127788.
[72] Y. Hou, H. Tang, B. Li, K. Chang, Z. Chang, X.Z. Yuan, H. Wang, Mater. Chem. Phys. 171 (2016) 137–144.
[73] J. Xiao, F. Zhang, K. Tang, X. Li, D. Wang, Y. Wang, H. Liu, M. Wu, G. Wang, ACS Cent. Sci. 5 (2019) 1937–1945.
[74] S. Tang, X. Zhang, Y. Sui, B. Wang, J. Li, L. Wu, Front. Chem. 8 (2021) 633949.
[75] X. Wu, J. Ma, Q. Ma, S. Xu, Y.S. Hu, Y. Sun, H. Li, L. Chen, X. Huang, J. Mater. Chem. A 3 (2015) 13193–13197.
[76] Y. Sui, Y. Hao, X. Zhang, S. Zhong, J. Chen, J. Li, L. Wu, Adv. Powder Technol. 31 (2020) 190–197.
[77] W. Qin, Y. Liu, J. Liu, Z. Yang, Q. Liu, Electrochim. Acta 418 (2022) 140357.
[78] H. Wang, B. Yang, X.Z. Liao, J. Xu, D. Yang, Y.S. He, Z.F. Ma, Electrochim. Acta 113 (2013) 200–204.
[79] T. Ma, G.L. Xu, Y. Li, B. Song, X. Zeng, C.C. Su, W.L. Mattis, F. Guo, Y. Ren, R. Kou, C. Sun, ACS Appl. Energy Mater. 1 (2018) 5735–5745.
[80] M. Palluzzi, L. Silvestri, A. Celeste, M. Tuccillo, A. Latini, S. Brutti, Crystals 12 (2022) 885.
[81] D. DiLecce, V. Marangon, M. Isaacs, R. Palgrave, P.R. Shearing, J. Hassoun, Small Methods 5 (2021) 2100596.
[82] M.H. Han, E. Gonzalo, N. Sharma, J.M. López del Amo, M. Armand, M. Avdeev, J.J. Saiz Garitaonandia, T. Rojo, Chem. Mater. 28 (2016) 106–116.
[83] H.R. Yao, P.F. Wang, Y. Wang, X. Yu, Y.X. Yin, Y.G. Guo, Adv. Energy Mater. 7 (2017) 1700189.
[84] Q. Liu, Z. Hu, M. Chen, C. Zou, H. Jin, S. Wang, Q. Gu, S. Chou, J. Mater. Chem. A 7 (2019) 9215–9221.
[85] L. Wang, J. Wang, X. Zhang, Y. Ren, P. Zuo, G. Yin, J. Wang, Nano Energy 34 (2017) 215–223.
[86] K. Wang, P. Yan, M. Sui, Nano Energy 54 (2018) 148–155.
[87] S. Komaba, N. Yabuuchi, T. Nakayama, A. Ogata, T. Ishikawa, I. Nakai, Inorg. Chem. 51 (2012) 6211–6220.
[88] Y. Wang, L. Wang, H. Zhu, J. Chu, Y. Fang, L. Wu, L. Huang, Y. Ren, C.J. Sun, Q. Liu, X. Ai, Adv. Funct. Mater. 30 (2020) 1910327.
[89] W. Zuo, J. Qiu, X. Liu, F. Ren, H. Liu, H. He, C. Luo, J. Li, G.F. Ortiz, H. Duan, J. Liu, Nat. Commun. 11 (2020) 3544.
[90] C. Xu, H. Cai, Q. Chen, X. Kong, H. Pan, Y.S. Hu, ACS Appl. Mater. Interfaces 14 (2022) 5338–5345.
[91] S.Y. Zhang, Y.J. Guo, Y.N. Zhou, X.D. Zhang, Y.B. Niu, E.H. Wang, L.B. Huang, P.F. An, J. Zhang, X.A. Yang, Y.X. Yin, Small 17 (2021) 2007236.
[92] X. Liang, Y.K. Sun, Adv. Funct. Mater. 32 (2022) 2206154.
[93] D. Zhou, W. Huang, X. Lv, F. Zhao, J. Power Sources 421 (2019) 147–155.
[94] L. Yang, J.M.L. del Amo, Z. Shadike, S.M. Bak, F. Bonilla, M. Galceran, P.K. Nayak, J.R. Buchheim, X.Q. Yang, T. Rojo, P. Adelhelm, Adv. Funct. Mater. 30 (2020) 2003364.
[95] S. Guo, P. Liu, H. Yu, Y. Zhu, M. Chen, M. Ishida, H. Zhou, Angew. Chem. Int. Ed. 54 (2015) 5894–5899.
[96] M. Bianchini, E. Gonzalo, N.E. Drewett, N. Ortiz-Vitoriano, J.M.L. del Amo, F.J. Bonilla, B. Acebedo, T. Rojo, J. Mater. Chem. A 6 (2018) 3552–3559.
[97] Y.N. Zhou, P.F. Wang, Y.B. Niu, Q. Li, X. Yu, Y.X. Yin, S. Xu, Y.G. Guo, Nano Energy 55 (2019) 143–150.
[98] C. Chen, W. Huang, Y. Li, M. Zhang, K. Nie, J. Wang, W. Zhao, R. Qi, C. Zuo, Z. Li, H. Yi, Nano Energy 90 (2021) 106504.
[99] G. Shanmugam, U.P. Deshpande, A. Sharma, P.M. Shirage, P.A. Bhobe, J. Phys. Chem. C 122 (2018) 13182–13192.
[100] Y. Li, M. Chen, B. Liu, Y. Zhang, X. Liang, X. Xia, Adv. Energy Mater. 10 (2020) 2000927.
[101] T. Hwang, J.H. Lee, S.H. Choi, R.G. Oh, D. Kim, M. Cho, W. Cho, M.S. Park, ACS Appl. Mater. Interfaces 11 (2019) 30894–30901.
[102] D. Zhang, X.M. Meng, Y.M. Zheng, X.M. Wang, S.D. Xu, L. Chen, S.B. Liu, Phys. Chem. Chem. 22 (2020) 19992–19998.
[103] K. Mathiyalagan, K. Karuppiah, A. Ponnaiah, S. Rengapillai, S. Marimuthu, Int. J. Energy Res. 46 (2022) 10656–10667.
[104] M. Kouthaman, P. Arjunan, K. Kannan, V. Priyanka, R. Subadevi, V. Kumaran, R.M. Gnanamuthu, M. Sivakumar, J. Taiwan Inst. Chem. Eng. 117 (2020) 86–92.
[105] M. Kouthaman, K. Kannan, P. Arjunan, T. Meenatchi, R. Subadevi, M. Sivakumar, Mater. Lett. 276 (2020) 128181.
[106] Q. Li, Y. Qiao, S. Guo, K. Jiang, Q. Li, J. Wu, H. Zhou, Joule 2 (2018) 1134–1145.
[107] Y. Zhang, M. Wu, J. Ma, G. Wei, Y. Ling, R. Zhang, Y. Huang, ACS Cent. Sci. 6 (2020) 232–240.
[108] W. Zheng, Q. Liu, Z. Wang, Z. Wu, S. Gu, L. Cao, K. Zhang, J. Fransaer, Z. Lu, Energy Stor. Mater. 28 (2020) 300–306.
[109] Y. Pei, S. Li, Q. Chen, R. Liang, M. Li, R. Gao, D. Ren, Y.P. Deng, H. Jin, S. Wang, D. Su, J. Mater. Chem. A 9 (2021) 2325–2333.
[110] Q. Zhang, Y. Huang, Y. Liu, S. Sun, K. Wang, Y. Li, X. Li, J. Han, Y. Huang, Sci. China Mater. 60 (2017) 629–636.
[111] H. Chen, Z. Wu, Y. Zhong, T. Chen, X. Liu, J. Qu, W. Xiang, J. Li, X. Chen, X. Guo, B. Zhong, Electrochim. Acta 308 (2019) 64–73.
[112] Y. Yu, D. Ning, Q. Li, A. Franz, L. Zheng, N. Zhang, G. Ren, G. Schumacher, X. Liu, Energy Stor. Mater. 38 (2021) 130–140.
[113] X. Xu, H. Huo, J. Jian, L. Wang, H. Zhu, S. Xu, X. He, G. Yin, C. Du, X. Sun, Adv. Energy Mater. 9 (2019) 1803963.
[114] D. Su, C. Wang, H.J. Ahn, G. Wang, Chem. Eur. J. 19 (2013) 10884–10889.
[115] X.H. Liu, W.H. Lai, S.L. Chou, Mater. Chem. Front. 4 (2020) 1289–1303.
[116] Q. Mao, R. Gao, Q. Li, D. Ning, D. Zhou, G. Schuck, G. Schumacher, Y. Hao, X. Liu, Chem. Eng. J. 382 (2020) 122978.
[117] D. Lu, Z. Yao, Y. Zhong, X. Wang, X. Xia, C. Gu, J. Wu, J. Tu, ACS Appl. Mater. Interfaces 11 (2019) 15630–15637.
[118] Y. Han, S. Heng, Y. Wang, Q. Qu, H. Zheng, ACS Energy Lett. 5 (2020) 2421–2433.
[119] L. Wang, P. Zuo, G. Yin, Y. Ma, X. Cheng, C. Du, Y. Gao, J. Mater. Chem. A 3 (2015) 1569–1579.
[120] T. Song, E. Kendrick, J. Phys.: Mater. 4 (2021) 032004.
[121] W. Kong, H. Wang, L. Sun, C. Su, X. Liu, Appl. Surf. Sci. 497 (2019) 143814.
[122] Y. Zhang, L. Liu, S. Jamil, J. Xie, W. Liu, J. Xia, S. Nie, X. Wang, Appl. Surf. Sci. 494 (2019) 1156–1165.
[123] L. Xue, S. Bao, L. Yan, Y. Zhang, J. Lu, Y. Yin, Front. Energy Res. 10 (2022) 847818.
[124] C. Shi, L. Wang, X.A. Chen, J. Li, S. Wang, J. Wang, H. Jin, Nanoscale Horiz. 7 (2022) 338–351.
[125] P. Gupta, S. Pushpakanth, M.A. Haider, S. Basu, ACS Omega 7 (2022) 5605–5614.
[126] S. Hwang, Y. Lee, E. Jo, K.Y. Chung, W. Choi, S.M. Kim, W. Chang, ACS Appl. Mater. Interfaces 9 (2017) 18883–18888.
[127] C. Lin, X. Meng, M. Liang, W. Li, J. Liang, T. Liu, X. Ke, J. Liu, Z. Shi, L. Liu, J. Mater. Chem. A 11 (2023) 68–76.
[128] J. Jayachitra, J.R. Joshua, A. Balamurugan, N. Sivakumar, V. Sharmila, S. Shanavas, M.A. Haija, M.W. Alam, A. BaQais, Ceram. Int. 49 (2023) 48–56.
[129] S. Xu, H. Chen, C. Li, R. Nie, Y. Yang, M. Zhou, X. Zhang, H. Zhou, Ionics 29 (2023) 1873–1885.
[130] S. Zhao, Q. Shi, R. Qi, X. Zou, J. Wang, W. Feng, Y. Liu, X. Lu, J. Zhang, X. Yang, Y. Zhao, Electrochim. Acta 441 (2023) 141859.
[131] S. Zhao, Q. Shi, W. Feng, Y. Liu, X. Yang, X. Zou, X. Lu, Y. Zhao, Chin. Chem. Lett. (2023) 108606.
[132] S.K. Gogula, V.A. Gangadharappa, V.K. Jayaraman, A.S. Prakash, Energy Fuels 37 (2023) 4143–4149.
[133] Q. Zhang, Z. Wang, X. Li, H. Guo, W. Peng, J. Wang, G. Yan, Chem. Eng. J. 431 (2022) 133456.
[134] K. Tian, H. He, X. Li, D. Wang, Z. Wang, R. Zheng, H. Sun, Y. Liu, Q. Wang, J. Mater. Chem. A 10 (2022) 14943–14953.
[135] C. Zhao, F. Ding, Y. Lu, L. Chen, Y.S. Hu, Angew. Chem. Int. Ed. 59 (2020) 264–269.
[136] B. Peng, Y. Chen, L. Zhao, S. Zeng, G. Wan, F. Wang, X. Zhang, W. Wang, G. Zhang, Energy Stor. Mater. 56 (2023) 631–641.
[137] V.R.R. Boddu, M. Palanisamy, L. Sinha, S.C. Yadav, V.G. Pol, P.M. Shirage, Sustain. Energy Fuels 5 (2021) 3219–3228.
[138] P. Wen, H. Shi, D. Guo, A. Wang, Y. Yu, Z.S. Wu, Renewables 1 (2023) 81–89.
[139] S.J. Kim, J.H. Hong, Y.C. Kang, Appl. Surf. Sci. 611 (2023) 155673.
[140] N.Q. Quyen, T. Van Nguyen, H.H. Thang, P.M. Thao, N. Van Nghia, J. Alloy. Compd. 866 (2021) 158950.
[141] F. Zhang, Y. Lu, Y. Guo, C. Li, Y. Liu, M. Yang, B. Zhao, W. Wu, X. Wu, Chem. Eng. J. 458 (2023) 141515.
[142] S. Deng, J. Luo, G. Zhao, B. Huang, Ceram. Int. 49 (2023) 18870–18877.

[143] A. Anilkumar, N. Nair, S.V. Nair, S. Baskar, J. Energy Storage. 72 (2023) 108291.
[144] B. Ouyang, T. Chen, X. Liu, M. Zhang, P. Liu, P. Li, W. Liu, K. Liu, Chem. Eng. J. 458 (2023) 141384.
[145] G. Su, H. Zheng, H. Chen, S. Bao, Mater. Lett. 331 (2023) S133425.
[146] F. Fu, P. Liu, H. Wang, Mater. Lett. 253 (2019) 124–127.
[147] S. Yuan, L. Yu, G. Qian, Y. Xie, P. Guo, G. Cui, J. Ma, X. Ren, Z. Xu, S.J. Lee, J.S. Lee, Nano Lett. 23 (2023) 1743–1751.
[148] J. Wang, S.L. Dreyer, K. Wang, Z. Ding, T. Diemant, G. Karkera, Y. Ma, A. Sarkar, B. Zhou, M.V. Gorbunov, A. Omar, Mater. Futures 1 (2022) 035104.